FINAL REPORT

Contract Number: *DTPH56-13-H-CAAP02*

Prepared for: *DOT*

Project Title: *Scaling and Self-Sensing in Composite Repairs of Corrosion Defects*

Prepared by: *The University of Tulsa*

Contact Information: *Michael W. Keller, mwkeller@utulsa.edu, 918-631-3198*

Executive Summary

The goal of the research presented in this report is to characterize two approaches for installing composite repairs intended for pressure equipment. Currently, the accepted composite pipeline repair is a full-encirclement repair installed in a continuous layer around the damaged region. The research presented in this report examines the performance of a discontinuous patch repair in lieu of a full-encirclement repair. The performance of these two repair types is examined by pressure fatigue testing on straight pipe samples of 6-inch nominal diameter. A 75% wall loss defect was machined into each sample to simulate external corrosion damage. Pressure was then cycled from 0 to maximum allowable operating pressure (MAOP) until either failure or runout of 100,000 cycles was reached. Fatigue lives and substrate strain levels are compared for the full-encirclement repairs and patch repairs. The average fatigue life for the full-encirclement repairs is 13,261 cycles with a standard deviation of 10,205 cycles while the patch repairs exhibited an average fatigue life of 51,852 cycles with a standard deviation of 42,363 cycles. Of the 18 samples tested, 9 were patch repairs and 9 were full-encirclement repairs. All full encirclement repairs exhibited a fatigue life less than 27,000 cycles. For patch repairs, 4 specimens reached runout of 100,000 cycles. The strain response of the full-encirclement and patch repairs indicated that at the beginning of fatigue cycling the patch repairs exhibited a larger strain in critical areas; however, at the end of fatigue life, the full-encirclement repairs exhibited a larger strain in the same critical areas. After the small-scale tests were completed, a large-scale vessel test was initiated. Patch repairs of the same design were installed on a 42-inch vessel and

cycled from 80 psi to 500 psi. The maximum pressure level was chosen to match the in-plane stresses present in the small-scale specimens. Based on the fatigue testing presented in this work, patch repairs are a viable solution for repairing pressure vessels and piping with external corrosion defects. Additionally, current results indicate that testing of repairs on small scale specimens is sufficient to determine repair success on larger scale pipe and pressure equipment.

1 INTRODUCTION

Pipelines in the United States of America are the primary mode of transportation for oil and natural gas, with over 400,000 miles of pipeline contained within the continental USA [1], [2]. The majority of these pipelines are over 40 years old and have begun to degrade due to age and environmental factors [3], [4]. Pipelines can be buried underground, left in open air, or a combination of the two, which promotes corrosion and metal degradation from oxidation or surface abrasion. As a result of this degradation, pipelines incur approximately $7 billion annually in repairs, with the bulk of the cost coming from traditional repair methods [3], [5]. Using traditional metallic repair approaches, a pipeline system must be taken offline for the damaged section of pipe to be replaced or sleeve-repaired. Shutting down pipelines increases the total cost of the repair by adding the lost operation time to the total expense.

The most common type of traditional repair is a sleeve repair, which requires circumferential access to the pipeline at the defect location. Installation of this repair type consists of either bolting or welding two halves of a steel sleeve around the damaged section. This sleeve then functions as an undamaged pipeline section. Replacement of the damaged section also requires circumferential access to the pipeline and involves cutting away the damaged section of pipeline to weld a new piece of pipeline in its place.

An alternative to these metallic repairs are fiber-reinforced polymer composites, also called fiber-reinforced plastics (FRPs). These repairs are bonded to a damaged pipe to restore the mechanical integrity of the substrate. Composite overwraps have three advantages over welded repairs: their conformability allows for installation in a wider range of geometries, they can be more cost-effective than traditional repairs because they can be applied while the system is online, and they can be less labor-intensive to install [6]. Over the last 16 years significant

research advances have increased the acceptability of FRP repairs in a wide variety of industries [7]–[11].

1.1 Fiber Reinforced Composites

Composite repairs consist of a thermosetting resin, such as an epoxy or polyurethane, with a continuous reinforcement fiber. Reinforcement geometries are typically one of two types: continuous unidirectional fiber or continuous woven fiber. Continuous unidirectional fibers are used for their superior uniaxial mechanical properties; however, these composites can require additional installation time because layers must be applied alternating the direction of the fabric to achieve a required axial strength. Woven fabrics tend to be the most common reinforcement architecture for pipeline repair because of their ability to add multi-axial strength in a single layer of reinforcement fabric.

1.1.1 *Generalized Installation of Composite Repairs*

The first step in composite repair installation is surface preparation. To ensure that the adhesion between the repair and the substrate is maximized, the damaged section of pipe typically undergoes a grit blasting process to remove any external buildup such as rust, paint, or dirt that may have gathered on the pipe while in use. This blast cleaning is generally recommended to be near-white, as described in the NACE-2 standard for surface preparation [12].

After blasting, the damaged section receives a solvent cleaning, usually with acetone or isopropyl alcohol, to remove any remaining dust or oily residues that can impair surface bonding between the substrate and the repair. Once the solvent has evaporated, dimensional restoration putty is used to fill in any corrosion damage and restore the substrate to its original external profile. After putty, a primer is typically applied to fill in any micro defects or cracks in the

substrate and promote adhesion between the composite and the steel. Figure 1.1 shows a damaged pipe section with putty applied (top, color pink) and with primer applied (bottom, color gray).

Figure 1.1: Damaged pipe section with restoration putty applied (top), the same damaged section with primer applied (bottom)

At this point, the substrate is ready for the composite material to be installed over the defect zone. The installation process begins with the saturation of the reinforcement fiber with the matrix material. Figure 1.2 shows this process, known as the wetout process, being completed where a paint roller is used to apply an epoxy matrix to a carbon fiber reinforcement.

Figure 1.2: Example of the wetout process. The epoxy is being spread onto a piece of carbon fiber using a paint roller [13]

After the reinforcement is saturated with the matrix material, the composite is ready for application. The wetted composite is wrapped around the previously prepared section. The process of wetout and application is repeated until the desired repair thickness is reached. A newly installed repair is frequently wrapped in a plastic stretch film to help consolidate the composite. After completing the installation, the composite is allowed to cure for a specified minimum duration, typically 24 hours. Once fully cured, the damaged section of pipe is considered repaired and ready to be returned to its fully operational online state. Figure 1.3 shows an example of a cured repair ready to be returned to its working state.

Figure 1.3: Example of a carbon composite repair installed on a damaged pipe section

1.1.2 Types of Composite Repairs

Nearly all composite repairs fall into one design category, full-encirclement repairs. These repairs consist of a circumferentially installed composite material over the damaged pipeline section, forming one continuous sleeve. This method has proven effective on smaller pipeline systems and is currently used for many applications in the oil and gas industry. However, as the diameter of a substrate increases, the amount of required composite material and labor necessary to install these repairs also increases. These factors combine to substantially increase the cost of a repair for large diameter substrates. Additionally, installing a full-encirclement repair on large diameter pressure vessels can become cumbersome.

One approach to reduce the increased cost of repairs installed on large diameter pressure vessels is to use patch repairs instead of full-encirclement repairs. Patch repairs consist of a *patch* of composite material bonded over the defect area. This type of repair is discontinuous around the substrate and can provide significant material and installation savings.

However, a lack of knowledge of the performance and strain response of patch repairs has

hindered widespread acceptance. Figure 1.4 shows a schematic representation of a full-encirclement and a patch repair.

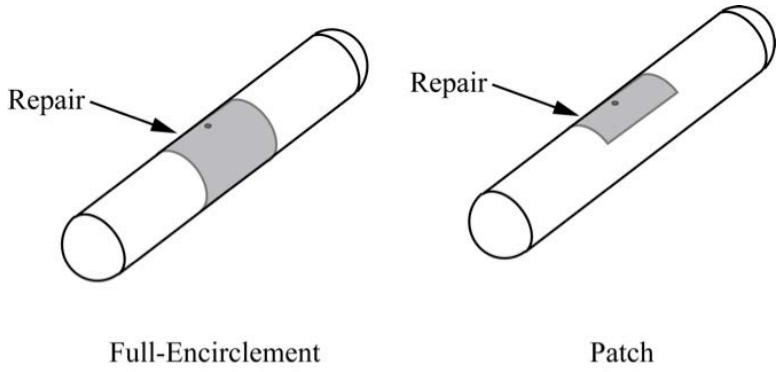

Figure 1.4: Two types of composite repair: full-encirclement repair (left) and patch repair (right)

1.2 Applicable Standards – ASME PCC-2

The American Society for Mechanical Engineers publishes ASME PCC – 2: Repair of Pressure Equipment and Piping that provides guidance for the design of composite repairs. This section discusses the design approach adopted by the standard for non-through wall defects as described in Part 4 of the standard. The equations below were based on the 2011 edition of the standard.

1.1.3 Thickness of Repair

The primary consideration for most repairs is the required thickness of the repair to restore the substrate to a desired pressure-carrying capacity. ASME PCC-2 provides design equations to determine minimum thickness requirements for composite repairs under certain applications. Equation 1 shows the thickness of repair design equation provided by industry standard. This thickness depends on the material properties of the composite material as well as

parameters of the substrate defect. This repair thickness is then broken down into individual composite layers based on the thickness of the individual reinforcement layers required to achieve the design repair.

$$t_{repair} = \frac{1}{\varepsilon_C E_C}\left(\frac{PD}{2} - st_s\right) \quad (1)$$

where: t_{repair} = design thickness of composite repair

ε_C = allowable circumferential strain in composite repair

E_C = Circumferential composite laminate tensile modulus

P = internal design pressure

D = external component diameter (outer diameter of substrate)

s = specified minimum yield strength (SMYS) of substrate

t_s = minimum remaining wall thickness of substrate

1.1.4 Extent of Repair, L_{OVER}

Aside from the required thickness of the repair, the minimum distance the repair must extend past the edges of the defect, L_{OVER}, is also a central design parameter for composite repairs. The current use of this parameter is to govern the axial distance the repair must extend past the edge of the defect, since the repairs are expected to be full-encirclement. This distance can be computed using either Equation 2 or Equation 3 depending on the available composite properties. Equation 2 is a function of the nominal outer diameter and the nominal thickness of the substrate. Equation 3 is to be used when the properties of the composite comply with ASME PCC-2 Article 4.1 Paragraph 3.4.6 regarding leaking components. Equation 3 uses material performance data such as tensile modulus, allowable strain, and lap shear strength to determine

L_{OVER} for different materials, allowing for better optimization of the extend of repair. For this study, L_{OVER} is adopted as the axial and circumferential extents for a patch repair. Finite element analysis is used in Section 2 to investigate this design choice. Adopting Equation 2 above, L_{OVER} is material property independent, which gives a value of 2.41 inches for the small-scale specimen used in this study and 6 inches for the large-scale specimen. To ensure installations met the required L_{OVER} Equation 4 was used post-installation.

$$L_{OVER} = 2.5\sqrt{\frac{Dt}{2}} \tag{2}$$

$$L_{OVER} = MAX\left(2.5\sqrt{\frac{Dt}{2}}\ or\ \frac{E_a \varepsilon_a t_{repair}}{\tau}\right) \tag{3}$$

where: L_{OVER} = length that the complete thickness of the repair must extend beyond damaged region (both axial and circumferential for patch repairs)

D = external component diameter (outer diameter of substrate)

t = nominal wall thickness of component (nominal pipe wall thickness)

E_a = tensile modulus for the composite in the axial direction

ε_a = allowable axial strain in composite repair

t_{repair} = design thickness of composite repair

τ = lap shear strength

$$L_{OVER,install} = \frac{L - l}{2} \tag{4}$$

where: $L_{OVER,install}$ = L_{OVER} installed over defect area.

L = total axial repair length (measured per installation)

l = axial length of the wall loss defect (l = 7.46 inches)

1.2 Research Goals

The primary goal of this research was to compare the performance of patch repairs to full-encirclement repairs under pressure fatigue loading. Results will help determine if patch repairs are a viable repair method for field applications. Data taken during this research program will help identify the need for design guidance revisions in industry standards.

In this report, chapter 2 will discuss the finite element analysis model and several trends that help explain underlying behaviors in the performance of these repairs. Chapter 3 will outline the experimental design including specimen manufacturing, test setup, and instrumentation. Chapter 4 will present results and discuss the experimental testing. Chapter 5 will provide conclusions for the performance of patch and full-encirclement repairs and suggestions for implementation of the results from this study.

2 FINITE ELEMENT ANALYSIS

In this chapter, the details and results of a computational analysis of patch and full-encirclement repairs will be discussed. These simulations serve to provide general trends that may apply for these types of repairs. Mesh convergence, percent wall loss, load cycle, Poisson ratio in the stress transfer material, and L_{OVER} simulations are described and results are evaluated in terms of expected repair performance.

2.1 Material Models and Simulation Metrics

The FEA model consisted of three components: a steel substrate, a composite repair, and dimensional restoration putty. Each of these components required material models to accurately represent physical results. The material model for both the composite and the putty were formed using experimental data provided from a previous composite repair research project [14]. The composite material was modeled as a linear-elastic orthotropic material with discrete properties applied to each of the hoop, axial, and out-of-plane directions. The dimensional restoration putty was modeled as an isotropic material [12]. The steel substrate material model was a multi-linear elastic plasticity model calibrated using quasi-static tensile tests performed using coupons cut from representative pipe sections [11]. Material data for all repair components can be found in appendix A.

All simulations consisted of a 0.25-inch thick composite layer bonded to the substrate. For these simulations, the composite repair was assumed to be perfectly bonded to the putty and the substrate. To meet PCC-2 requirements repairs extended a minimum of 2.41-inches in the axial direction beyond the edge of the defect [14]. Figure 2.1 shows L_{OVER} for both the hoop and axial directions.

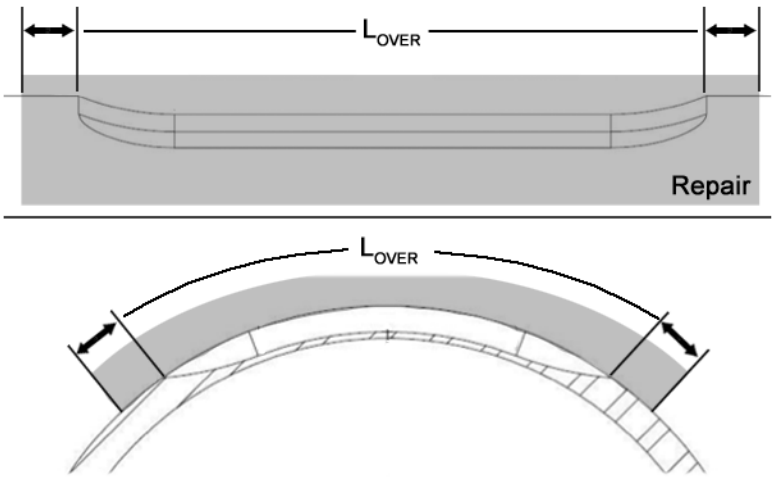

Figure 2.1: L_{OVER} for both hoop and axial directions

The internal pressure for the FEA simulations was set to the maximum allowable operating pressure (MAOP) of the substrate pipe. MAOP is defined as 75% specified minimum yield strength (SMYS) and is 2,130 psi for 6-inch ASTM schedule 40 steel pipe. This pressure was applied to the interior surface of the modeled pipe including the weld cap at the end of the pipe section.

Each simulation was meshed using hexagonal elements with a refined mesh in the defect area. Through thickness seeds were set at a minimum of 5 elements through the substrate and 10 elements through the composite and putty. The complexity of the defect transition geometry from the hoop to the axial direction required a swept advancing front technique with hexagonally dominated elements instead of hexagonal elements. Changing element type allowed for minimal use of tetrahedral elements for proper meshing. This condition was applied only in the defect transition (inset view of Figure 2.2, shown in yellow). Each simulation was run using non-reduced integration methods. Detailed images of the mesh can be found in Appendix B.

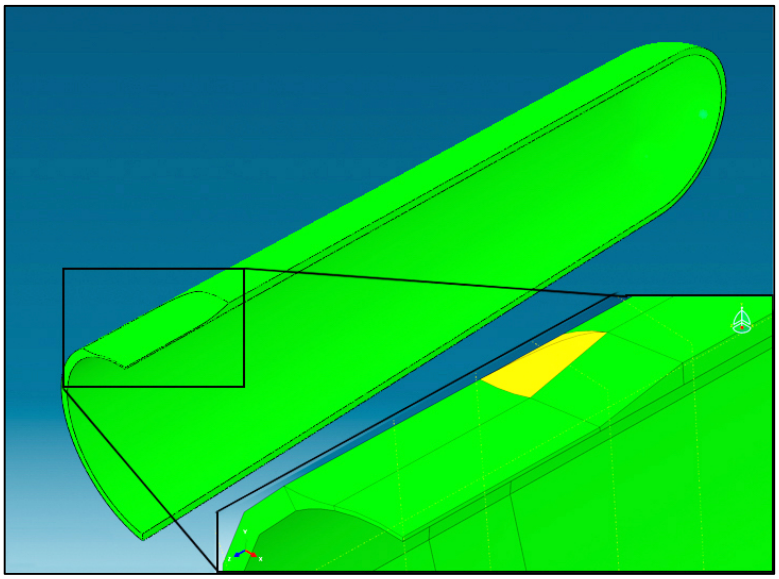

Figure 2.2: Simulation model with enlarged defect section

As seen in Figure 2.2 only ¼ of the pipe was modeled for each simulation. The symmetric nature of the geometry allowed for symmetric boundary conditions to be used reducing the simulation complexity and increasing computational efficiency.

2.2 Mesh Convergence Study

A mesh convergence study was performed to optimize simulations and determine the required regional mesh density. This study consisted of applying a finer mesh globally over the entire pipe section first, then locally at the defect location until the max principal stress values remained essentially constant between refinement steps. Stress values were taken at the same location after each refinement and compared to previous values. Figure 2.3 shows a graph of the element size vs. max principal stress for each mesh refinement.

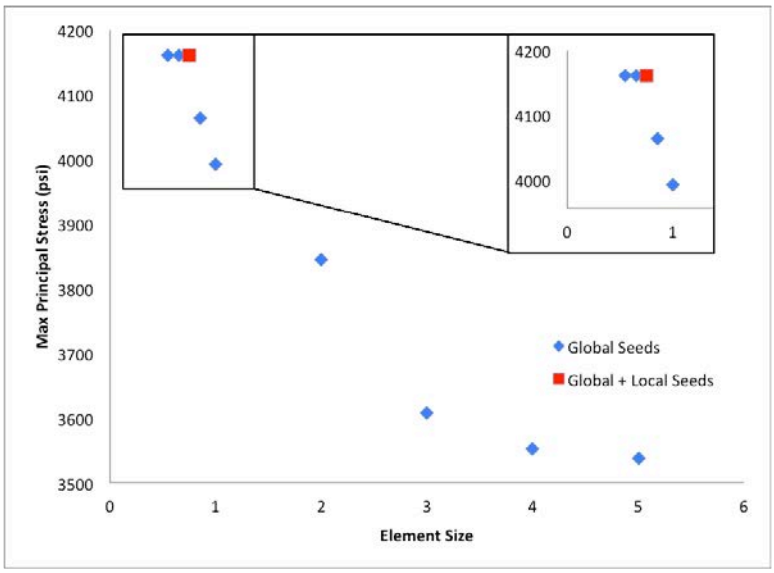

Figure 2.3: Max principal stress vs. mesh seed size for both global seeding and combined seeding

As shown in the inset of Figure 2.3, the constant max principal stress value reached during the mesh convergence was 4160 psi and occurred at a seed size of 0.75 and remained constant for all seed values less than 0.75.

To optimize the model and reduce computational time an additional study was performed using global seeds of 2.5 and locally refining the mesh at the defect with a seed size of 0.75. This additional sub-study yielded the same stress results but with a significant decrease in computation time. At this refinement level, the mesh was deemed acceptable for the FEA studies and was used for all studies henceforth. appendix C tabulates the mesh convergence data.

2.3 Wall Loss Study

Three parameters, stress in the substrate, strain in the composite, and repeatability of machinability were considered when defining an optimal percent wall loss to simulate corrosion damage. Stress levels in the substrate were assessed at the most severe location, the edge of the

defect just before the machined radius. Strains in the composite were also assessed at the most severe location, top center of the defect. This study helped gain understanding of the behavior of full-encirclement and patch repairs. The data used in the following sections is tabulated in appendix D.

2.3.1 Substrate Stress Level

To understand the influence of the wall loss on the strain in the damaged region of the substrate pipe, a series of simulations were run varying the percent wall loss from 50% to 80%. Figure 2.4 shows the results of these simulations.

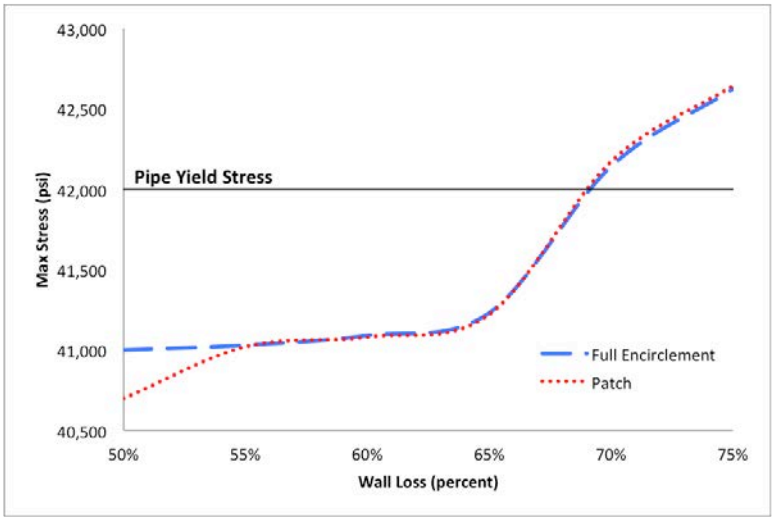

Figure 2.4: Max stress vs. percent wall loss in the substrate for full-encirclement and patch repair types

Analysis of the computational data indicates that percent wall loss greater than 70% will experience plastic deformation. Yield of the substrate is important, as this is the point at which significant load transfer to the composite begins to occur. As expected, as percent wall loss increases, stresses in the defect also increase for both the full-encirclement repair and patch

repair. For this analysis, the patch geometry has little to no effect on the stresses developed in the substrate at percent wall loss values greater than 55%. However below 50% wall loss the substrate stresses diverge with the full-encirclement repair maintaining a larger stress than the patch repairs. Based on the strain and stress levels in the substrate, the patch and full-encirclement repairs should have similar behavior.

2.3.2 Repair Strain Level

From the wall loss simulations, the max stress and strain in the repair was extracted. Figure 2.5 shows the strain level in the composite repair vs. percent wall loss.

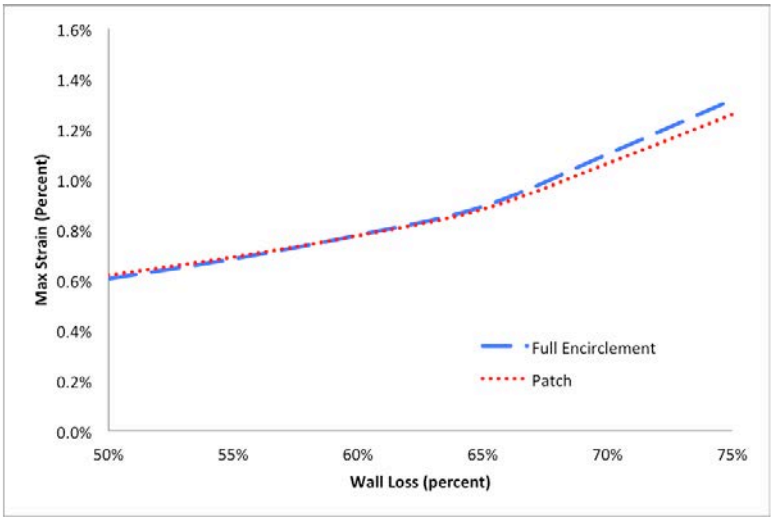

Figure 2.5: Max Strain vs. percent wall loss in the composite repair for full-encirclement and patch repairs

Strain in the composite exhibits similar trends as the stresses in the substrate. As expected, as the percent wall loss increases, the strain is transferred to the composite and the max strain in the composite increases. Unexpectedly, the full-encirclement repair strain is greater than the patch repair strain as the wall loss increases. At 75% wall loss, the strain in the full-encirclement repair is 4.51% difference greater than the strain in the patch repair.

This phenomenon is likely a result of the way in which the repair adds strength to the substrate. A full-encirclement repair provides reinforcement to all sides of the composite while the patch repair only provides strength over the defect area. When a load is applied the full-encirclement repair must bear the stress in the pipe circumferentially, not allowing for the undamaged substrate to expand under load. The nature of the patch repair allows for the substrate to expand under load and release some load at the top of the repair. This is a likely cause for the elevated strain levels in the full-encirclement repair. Figure 2.6 shows deformed shapes from the FEA model.

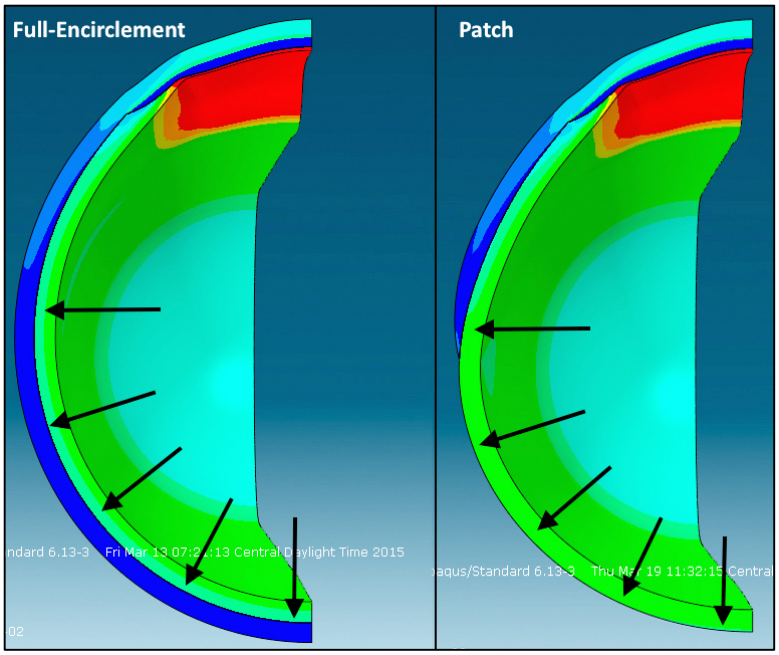

Figure 2.6: Comparison of deformation under load for full-encirclement (left) and patch repairs (right)

2.4 Pressure Cycle Study

To better understand the strain response of the composite repair under fatigue loading, a pressure cycle was simulated in FEA. These simulations were run using substrates with of 75% wall loss. Pressure amplitude was increased from 180 psi to 2,130 psi (MAOP) during this simulation. The results of this simulation are shown in Figure 2.7.

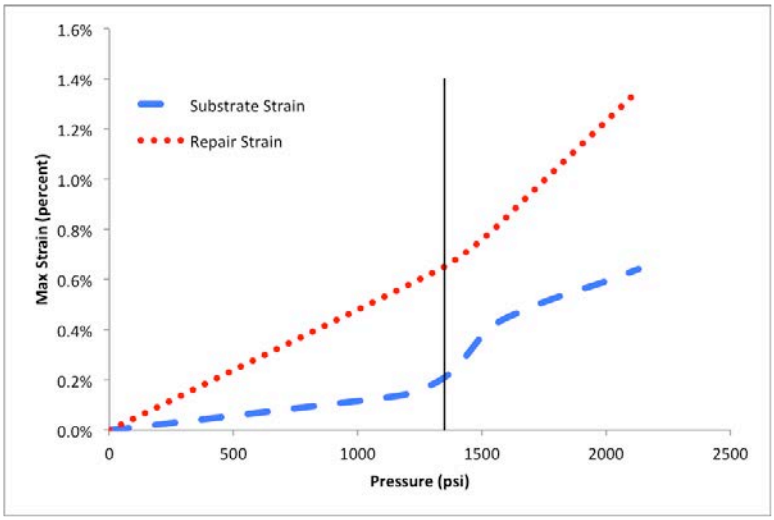

Figure 2.7: Max Strain vs. pressure for one full pressure cycle

As expected an increase in pressure results in an increase in strain for both the substrate and the composite repair. An interesting result that initiated further investigation is the location indicated in Figure 2.7 as onset of yielding. At this point, approximately 1400 psi, the steel substrate begins to plastically deform in the defect area. Prior to this simulation, the composite repair strain was expected to increase as soon as the plastic deformation of the substrate began. However, examination of the data indicates that load transfer began after significant plastic deformation. This unexpected lag in load transfer lead us to question whether the restoration putty modeled in the simulation causes a delay in strain transfer to the composite. This lag time could be caused by compressibility of the putty, where compressibility of the putty delays load

transfer to the composite. The role of the load transfer putty is discussed in greater detail below.

2.5 Bulk Modulus Study

Based on the observation of delayed load transfer, we hypothesized that reduced compressibility would improve load transfer. This was accomplished by varying the bulk modulus of the putty. Bulk modulus was varied by fixing the elastic modulus and varying the Poisson ratio from 0.25 to 0.48. The lower bound was chosen based on experimental data provided by an external partner whose putty has a Poisson ratio of 0.28 and the upper bound was chosen based on restriction in computational stability of the FEA tool used. Figure 2.8 shows a maximum strain value in the composite vs. the computed bulk modulus [13].

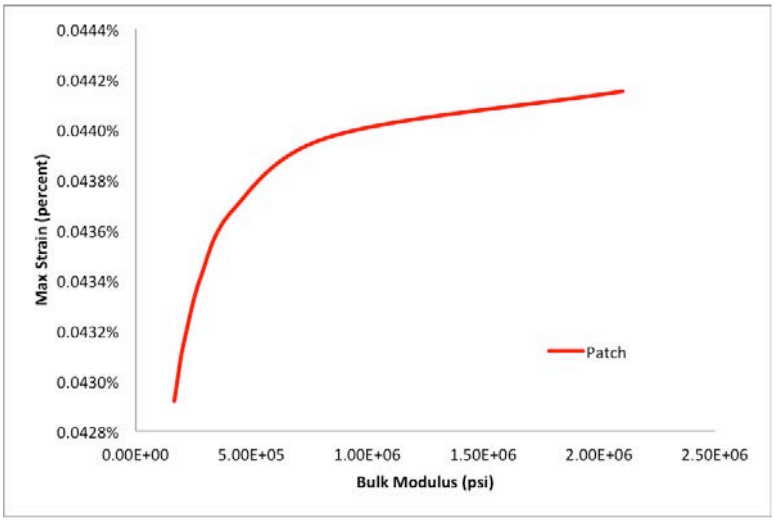

Figure 2.8: Max strain vs. bulk modulus for a patch repair

From this study, it can be concluded that increasing bulk modulus leads to increased repair strain, however the variation in that strain is small, 0.00123% from a Poisson ratio of 0.25 to 0.48. This indicates that Poisson's ratio and subsequently, bulk modulus, have little effect on the load transfer capability of the putty. This result is further confirmed by Figure 2.9.

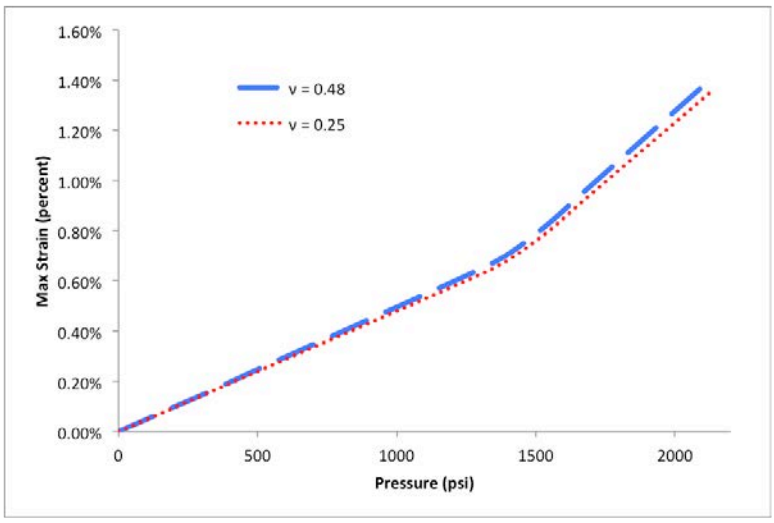

Figure 2.9: Max Strain vs. pressure for varied Poisson ratios

Another pressure cycle simulation was run using Poisson ratios of 0.25 and 0.48. These results confirm the slight increase in maximum strain as Poisson ratio increases, but the inflection point in Figure 2.9 falls at the same location for both Poisson ratios. This result indicates that compression of the load transfer putty has little impact on the onset of load transfer.

2.6 Extent of Repair, L_{OVER}, Study

The extent of repair, also known as L_{OVER}, is the minimum specified distance a repair must extend past the damaged section of pipe as specified by the ASME PCC-2 standard [14]. L_{OVER} is particularly important for patch repairs because the performance of the repair relies heavily on the bonding between the substrate and the composite material. In contrast, full-encirclement repairs can rely on the laminate bonding as well as the surface bonding for its strength.

For a 6-inch standard wall pipe L_{OVER} is 2.41-inches. In this study, L_{OVER} was varied from 2.4 to 12 inches to determine the influence of extent of repair on the overall repair. Figure

2.10 graphically shows the results of this study.

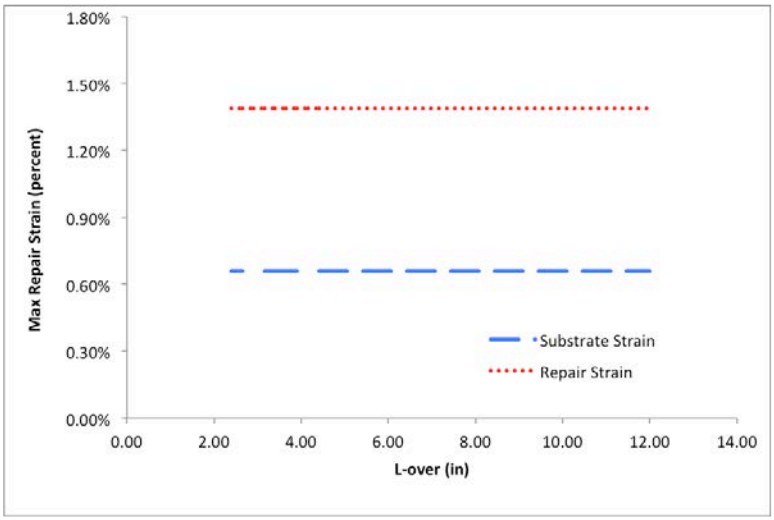

Figure 2.10: Max repair strain vs. L_{over}

As indicated in Figure 2.10, L_{OVER} exceeding the minimum bound appears to have no effect on the strain developed in the repair. This is likely a result of the assumed perfect bonding between substrate and repair made for these FEA studies.

3 EXPERIMENTAL

Full scale fatigue testing was run to characterize the performance of patch and full-encirclement repairs. This chapter describes sample design, sample manufacturing, basic repair installation metrics, fatigue testing, and instrumentation.

3.1 External Participation

To better replicate real world composite repairs, three external pipeline repair companies installed the composite repairs used in this testing. This allowed for a more realistic install by removing errors that may arise having a novice perform the installation. The three external pipeline repair companies who participated in this research are henceforth designated as Company A, Company B, and Company C. Each company was asked to install a total of 6 composite repairs, 3 full-encirclement and 3 patch repairs. To preserve consistency across repair types, they designed one full-encirclement repair compliant with ASME PCC-2 and simply created a discontinuity to create the patch repairs allowing for a true comparison of repair types. Approaches varied among companies with each company using their own proprietary repair techniques.

3.2 Sample Preparation & Manufacturing – Small Scale Testing

3.2.1 Specified Pipe Material

ASME PCC-2 specifies minimum criteria for quasi-static pipe testing as a part of the minimum performance testing. Minimum requirements include: a pipe diameter of 6-inches and a minimum length of 6 times the diameter plus the repair. This sample was used as the basis for the fatigue testing. Dimensions are provided in Table 1.

Table 1: Required sample dimensions as defined by ASME standard

	Pipe Dimensions (inch)
ID	6.065
OD	6.625
Wall Thickness	0.280
Length	48

The same standard requires that the test pipe should have a SMYS of 35,000 psi and local availability dictated that samples be manufactured from ASTM A106 Grade B pipe. Mill test reports indicate that the actual yield strength of the pipe to be 42,000psi.

3.2.2 Axial and Hoop Dimensions

The sample defects were designed according to the requirements outlined in Mandatory Appendix III in ASME PCC-2. These testing guidelines specify minimum requirements for the axial and hoop lengths of a machined wall loss defect [15]. From this criteria, minimum axial and hoop dimensions were calculated to be 6.625 inches and 3.3125 inches respectively. To reduce stress concentrations at the edges of the defect, a filet radius of 3 inches was added to borders of the defect area. Figure 3.1 shows a dimensioned schematic of the defect with a side view of the axial dimensions (top) and a front view of the hoop dimensions (bottom).

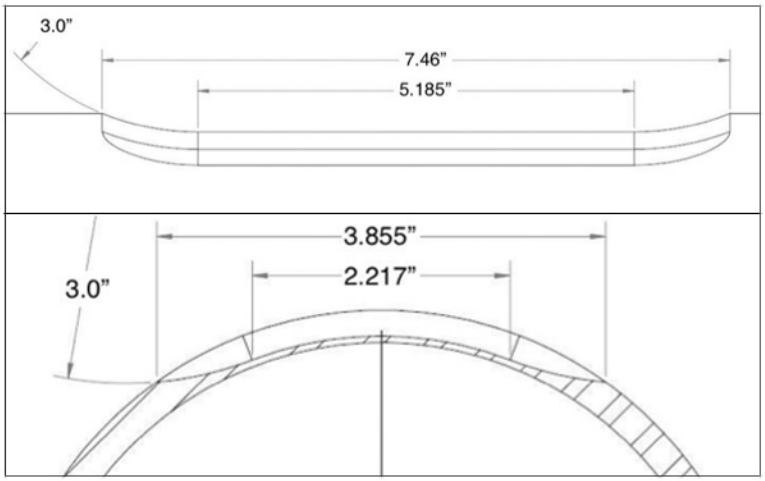

Figure 3.1: Defect dimensions as indicated by PCC-2

3.2.3 Percent Wall Loss

According to the standard "The Repair System supplier can select the depth of the defect, i.e., percentage of wall loss" indicating that the percent wall loss can be chosen to fit the needs of the test [15]. To determine this wall loss percentage, a study of the physical limits of the available CNC equipment was conducted. Several test runs indicated that a 75% wall loss defect was the most replicable and most consistent machined defect.

3.2.4 Machining of Test Specimen – small scale

Test samples were CNC machined at The University of Tulsa's McElroy Prototyping Laboratory from 6-inch diameter, schedule 40 ASTM A106 Grade B (x42) straight pipes. Each sample was machined using a 1-inch ball end-mill to aid in the accurate replication of filet radii. Figure 3.2 shows the resulting machined defect. Additionally, appendix E tabulates the thickness measurements after the machining process for test specimens in this study.

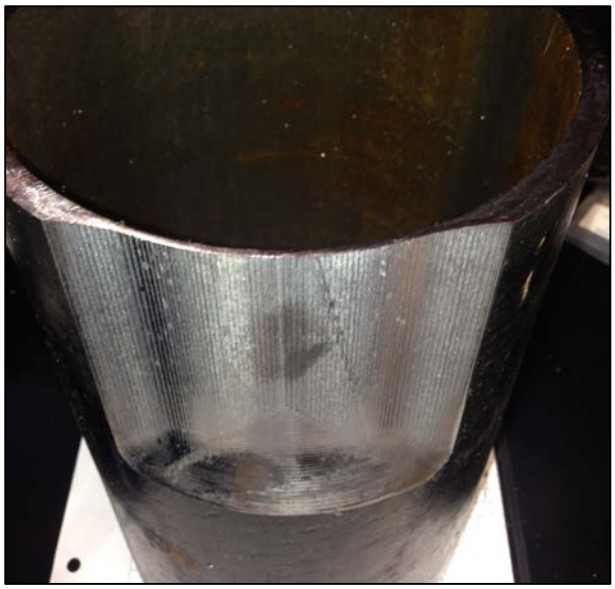

Figure 3.2: Cross section of defect immediately following CNC machining

Hemispherical end caps were then welded to each end of the pipe as well as an inlet and outlet coupling. Figure 3.3shows the final weld diagram for each test sample.

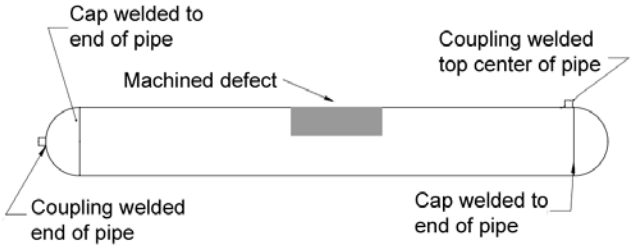

Figure 3.3: Schematic of each pipe specimen including weld locations

3.3 Sample Preparation & Manufacturing – Large Scale Testing

The initial project was planned to use a donated 60-inch test vessel for the large-scale test phase of this research. Unfortunately, prior to the start of this testing phase, those test vessels were scrapped and were unavailable. As a replacement, a 42-inch vessel was fabricated locally

to replace those scrapped vessels. The replacement vessel was fabricated using rolled and welded flat A36 steel sheets with defects that were machined prior to welding. A schematic of the pressure vessel is shown in Figure 3.4.

Figure 3.4: Schematic overview of large-scale (42'' diameter) pressure vessel.

Defects that were nominally similar to the defects produced for the small-scale specimens were pre-machined into flat plates as shown in Figure 3.5.

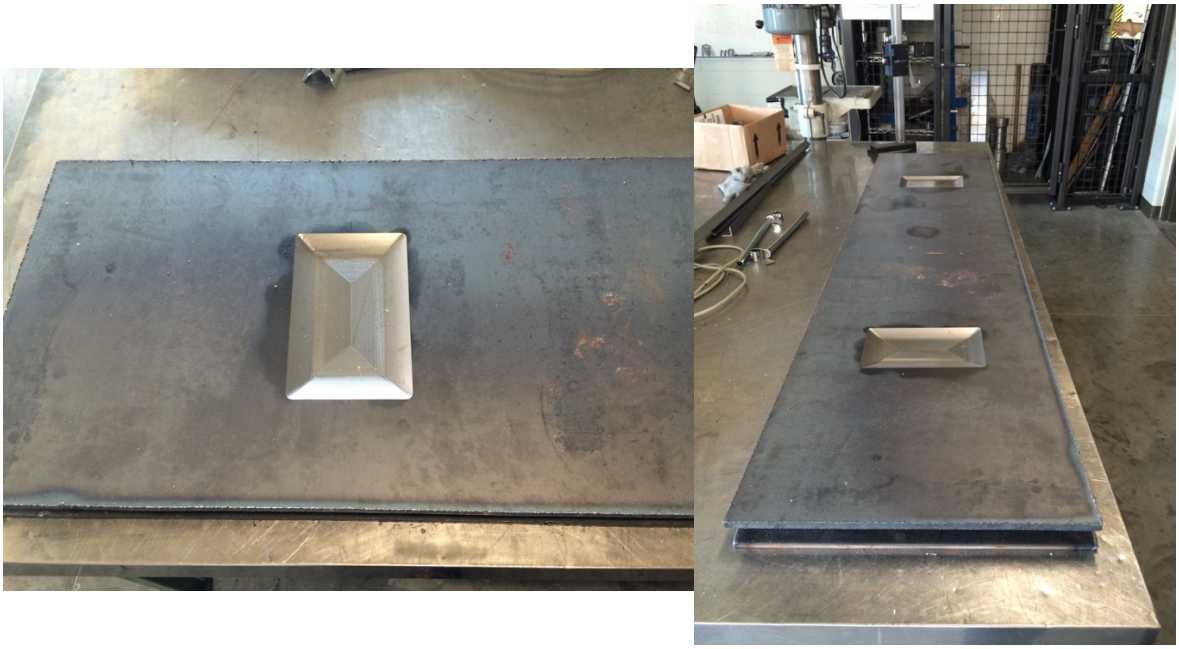

Figure 3.5: Images of machined flaws in plate prior to rolling and welding.

Figure 3.6: 42-inch vessel with installed patches.

Test pieces were first rolled to ensure that the rolling process would not distort the defect significantly. After this test demonstrated that this was a viable fabrication approach, the full vessel was fabricated and the participants installed repairs on the test vessel. The completed vessel with installed repairs is shown in Figure 3.6.

3.4 Fatigue Testing

In this section the test setup and instrumentation, when appropriate, are discussed for both the large scale and the small-scale tests. Unless noted, test procedures were the same for both small and large scale testing.

3.4.1 Flow Loop

A single vessel fatigue system was used to pressure cycle the repaired test specimens from 0 psi to 2,130 psi at an average rate of 24 cycles per minute. Large scale specimens were cycled to 500 psi, which gave an in-plane stress similar to that of the small-scale specimens. A schematic of the flow diagram is shown in Figure 3.7.

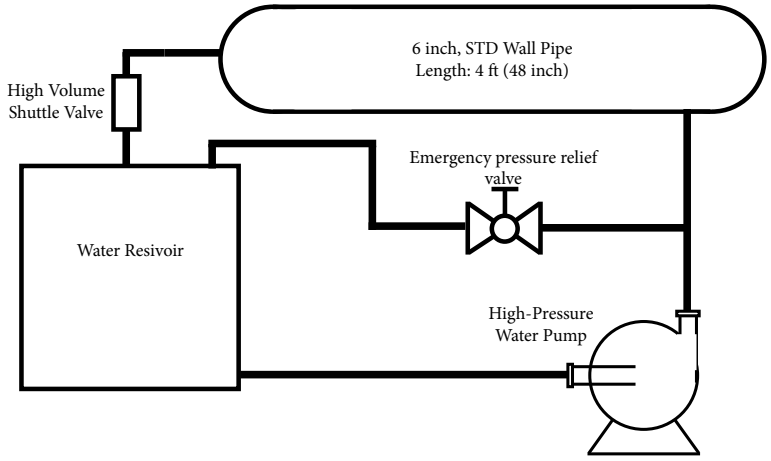

Figure 3.7: Fatigue flow loop used for testing

Each pipe was filled with water and care was taken to ensure all air was removed from the system. Once filled, the high-pressure system was brought online, the pressure relief valve was closed, and fatigue cycling began. Each pipe was tested in the same location and was securely supported on either end away from the repaired defect to minimize any environmental influence.

3.4.2 Control System

Simplicity of design was a major consideration in the control system for this fatigue setup. The control box consisted of a pressure switch that controlled the set point test pressure. This switch controlled the switching side of an electromechanical relay and the switch side controlled a high flow solenoid value and a counter. The high-pressure water pump would apply pressure, once the set point pressure was reached the pressure switch actives the relay, applying power to the solenoid and opening a drain valve. When the pressure in the pipe reached a reset point, approximately 50 psi, the solenoid valve closed and the process restarts. An analog counter was wired to trigger each time the solenoid valve switched providing a cycle counter for

fatigue loops. An additional output signal was wired in later and used to trigger a LabVIEW program to take data. LabVIEW and data acquisition will be covered in the next section

3.5 Instrumentation

Internal pressure, strain, and cycles to failure were recorded using a LabVIEW-based computerized data acquisition system. Additionally, cycles to failure were also recorded for all samples via an analog counter wired directly to the solenoid valve within the control box.

3.5.1 Cycle Counting

Cycle counting was performed for all 18 samples via an analog counter wired to count a cycle only when the solenoid valve engaged. This setup was more reliable than a computer-based system reading data and identifying peaks. Figure 3.8 shows a simplified schematic of the control box used during testing.

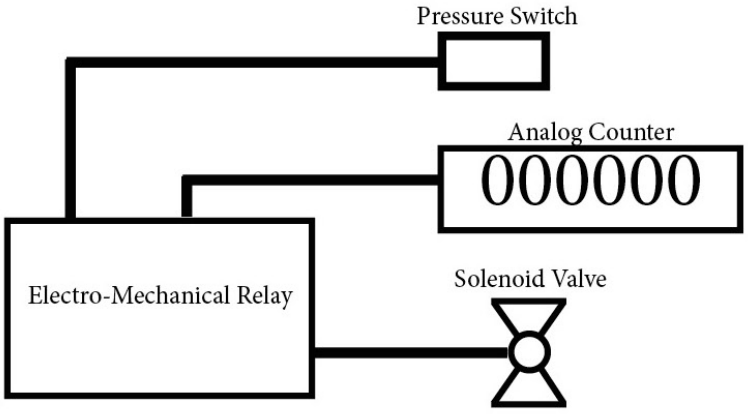

Figure 3.8: Schematic of the control box used during testing

At the beginning of each test the counter was reset to zero before the test program began. At the end of test each day, the cycles were recorded to ensure no loss of data. The counter was

not reset again until either failure or runout was reached.

Cycles were also counted via LabVIEW for the samples that were instrumented with strain gauges. A digital signal was taken from the control box and used as an input to LabVIEW. This signal triggered the computer to record a data point and each trigger was counted as 1 cycle. Cycles were counted and compared to analog counting and found to be slightly different. LabVIEW counted on average 23 more cycles per test sample than the analog counter. Further investigation indicated that digital signal noise was causing additional cycle triggers. These additional cycles were discarded.

3.5.2 Strain Gauges – Small Scale specimens

Of the 18 small-scale pipes repaired and tested, 6 were instrumented with strain gauges and strain was recorded for the duration of the fatigue testing. Strain gauges were applied to one patch and one full-encirclement repair from each company. Gages were installed in several locations including the surface of the defect, the external surface of the repair, the substrate, and in the discontinuous section of the repair (patch samples only). A complete map of strain gauge installations is shown schematically in Figure 3.9.

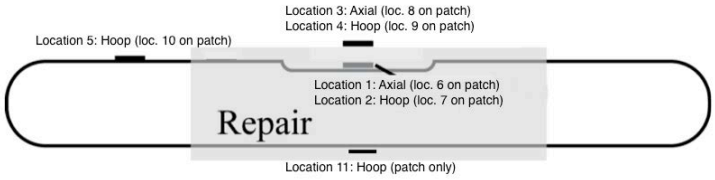

Figure 3.9: Schematic of strain gauge locations

The strain gauges on the surface of the defect (gauge locations 1 and 2) were installed prior to repair installation and measured strain in both the hoop and axial directions. Wire leads for these gauges were 30-gauge, 3-conductor flat wire. The wire was secured such that it had minimal effect on the performance of the repair. An example of a strain gauge installed on the

defect surface under the composite repair is shown in Figure 3.10. Strain gauges applied on the external surface of the repair were also measuring strain in both the hoop and axial directions. The substrate and discontinuous section on the patch repair both measured strain in the hoop direction only.

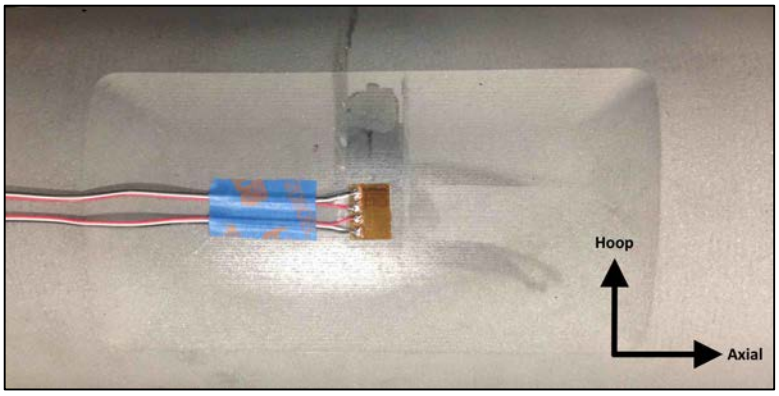

Figure 3.10: Example of a strain gauge installed on the defect surface

The strain gauges installed on the external surfaces of the repair were installed after the repair had been allotted a minimum 24-hour cure time. Additionally, gauge wires were cut to the same length and properly secured according to supplier recommendations.

Two types of strain gauges were used in this testing. Both hoop and axial strain were of interest in this testing for the defect and the composite, while only hoop strain was of interest for the substrate. Single axis and bi-axis gauges were used for testing and are shown in Figure 3.11 with dimensions. The biaxial gauges were selected such that they would cover a large enough composite area to accurately represent the strain in that location. Each gauge was 350-Ω nominal resistance with 10-volt excitation. Gauges were each connected with 3-foot 30-gauge wire to a National Instruments 9945 quarter bridge 350-Ω completion adaptors. Bridge adaptors were then connected to one of three NI 9237 analog input modules via RJ50 cable. A single National Instruments 8-module chassis was used to connect analog input modules for strain and pressure

readings and a NI 9401 module was used to input a digital signal from the control box to trigger cycle counting.

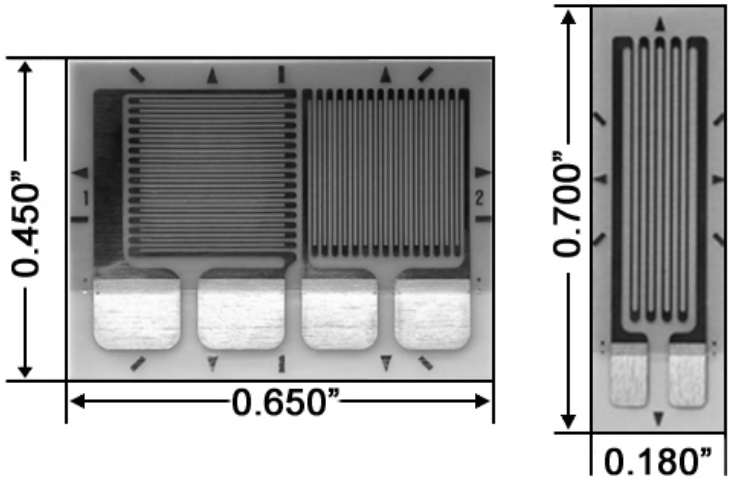

Figure 3.11: Strain gauges used for testing

3.5.3 Data Acquisition System

A LabVIEW program was used to measure strain, pressure, and count cycles for 6 of the 18 specimens. This program was triggered via a digital signal coming from the fatigue control box. Upon triggering, LabVIEW would read a measurement from each strain gauge, the pressure sensor, and add a cycle to the counter. LabVIEW was also programed such that every 200 cycles 4 full pressure loops were recorded. These cycles were monitored to ensure the system was pressure cycling properly and that all strain gauges were active. Figure 3.12 shows an example of the gathered loop data.

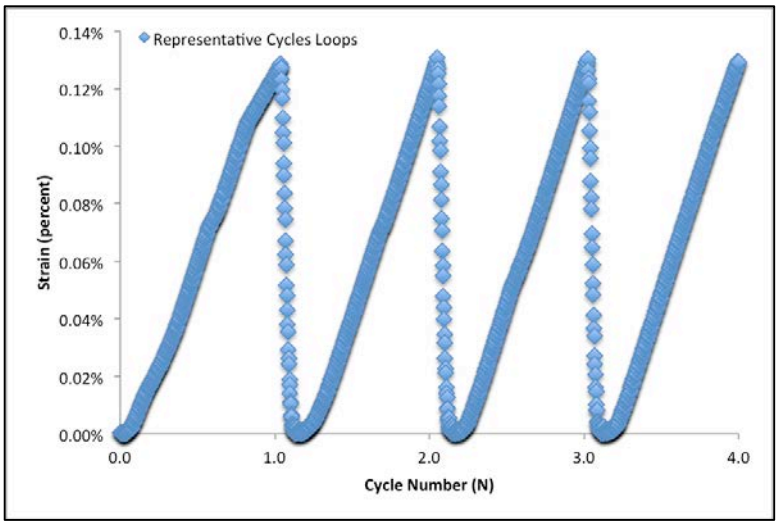

Figure 3.12: Example of complete strain cycle loops

Figure 3.12 shows that the pressure cycles are in the form of a ramp with the pressure load being applied at a much slower rate than depressurization.

3.6 Repair Installation

Repair design varied between companies with each company using its own proprietary materials. Table 2 shows a general breakdown of the repair materials.

Table 2: General repair metrics per company

	Reinforcement Material		Thermoset Material
	Hoop Direction	Axial Direction	
Company A	Fiberglass	Fiberglass	Polyurethane
Company B	Carbon Fiber	Carbon Fiber	Epoxy
Company C	Carbon Fiber	Fiberglass	Epoxy

Variation in composite material required differences in the design of the repair to satisfy testing standards. The two major differences in the repairs were thickness and L_{OVER}. Table 3

tabulates the overall thickness of the repair and the number of reinforcement layers applied to achieve that thickness.

Table 3: Thickness of repair per company

	Number of Layers in Repair		Thickness of Repair, t_{repair} (inch)
	Full-Encirclement	Patch	
Company A	36	36	0.85
Company B	9	9	0.169
Company C	18	18	0.440

To ensure each company met or exceeded standard requirements Equation 4 was used with physical measurements from each pipe. Table 4 tabulates the average L_{OVER} per company.

Table 4: Average L_{OVER} per company

	Average L_{OVER} Measured (inches)	
	Full-Encirclement	Patch
Company A	2.874	2.853
Company B	2.853	2.833
Company C	6.978	7.645

Based on field measurements all three companies met or exceeded the minimum specified extend of repair. Companies A and B exceeded the minimum by just under 0.5 inches each while company C exceeded the minimum by more than 4 inches.

4 EXPERIMENTAL RESULTS

Fatigue testing was performed on 18 pipes, 9 with patch repairs and 9 with full-encirclement repairs. Of those 18 pipes, 2 pipes from each participating company (6 pipes total) were instrumented with strain gauges for the duration of testing. Digital image correlation (DIC) was used to capture full-field strain data for a single load cycle. This chapter discusses the results of fatigue data, DIC, and strain data.

4.1 Small Scale Fatigue Results – Cycles to Failure

Cycles to failure were recorded for all test samples via an analog counter mounted in the control box as described in chapter 3. Failure was defined as the cycle during which water penetrated the composite repair. Testing experienced two types of failures, pinhole failures through the composite repair and delamination failures from the substrate. There were 8 delamination failures, 6 pinhole failures, and 4 pipes that reached runout of 100,000 cycles. Table 5 tabulates the quantity each failure mode by company. Figure 4.1 graphically depicts the cycles to failure for each test specimen. This fatigue data and computed t-test statistics is also tabulated in appendix G.

Table 5: Failure mode based on company

	Failure Mode		Runout
	Delamination	Pinhole	100,000 +
Company A	4	2	0
Company B	2	2	2
Company C	2	2	2

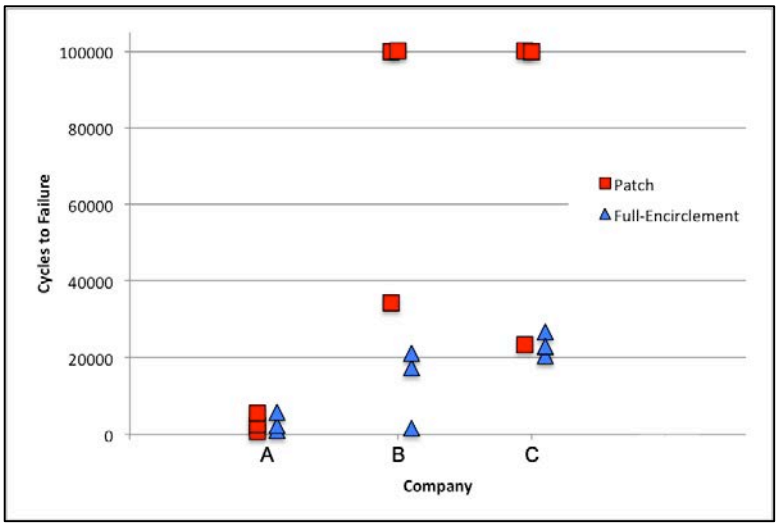

Figure 4.1: Cycles to failure vs. participating company

Each repair installed by Company A failed before 6,000 cycles. The maximum cycles to failure was 5,798 cycles and occurred on a full-encirclement repair while the minimum cycles to failure was 748 cycles and occurred on a patch repair. The average cycles and standard deviation of Company A was 2,989 cycles and 2,033 cycles respectively, giving Company A the lowest standard deviation and lowest average cycles to failure. A standard 2-tailed t-test, using a 95% confidence interval, was performed on the data and indicates that the patch repair and the full-encirclement repair are statically similar from one another with a p-value of 0.993.

Companies B had interesting fatigue life results with 2 of the patch repair samples reaching runout and one of the full-encirclement repairs failing at 1,605 cycles making these values the maximum and minimum values of for Company B. Two unexpected results included a patch repair sample, which failed at 34,286 cycles and a full-encirclement repair, which failed at 1,605 cycles. These samples had strain gauges applied and exhibited failure along the strain gauge wires. Application of the strain gauges on the surface of the defect likely caused a decrease in repair strength resulting in premature failure for these two specimens. The average

cycles to failure for Company B is 45,736 cycles with a standard deviation of 39,532 cycles. A standard t-test performed on the data indicates that, with 95% confidence, the full-encirclement repair and the patch repair are statistically similar with a p-value of 0.089.

Company C had similar results to Company B in that two of the patch repairs reached runout while one failed at 23,371 cycles through the strain gauge wires. Again, this indicates that the applied strain gauge decreased the repair strength causing premature failure. Company C had an average cycles-to-failure and standard deviation of 48,933 cycles and 36,155 cycles respectively. Simple t-test results indicate that the full-encirclement repair and patch repair are statically similar with a p-value of 0.117.

It is expected that if this testing was repeated and strain gauges were not applied to the defect area the cycles to failure would be conclusive that the patch repair and full-encirclement repairs would be statically different with the patch repair surviving longer than the full-encirclement repair. Average cycles to failure for the patch repair was 51,852 cycles with a standard deviation of 42,363 cycles while the average cycles to failure for the full-encirclement repairs was 13,261 cycles with a standard deviation of 10,205 cycles. Performing a t-test on all 18 repaired types to compare full-encirclement and patch repairs supports this expectation and results that the patch repair is statistically different from the full-encirclement repair with a p-value of 0.0398. Fatigue cycles to failure indicate that patch repairs are a viable solution for repairing corrosion defects on 6-inch diameter pipeline.

A post-installation report from each company aided in the evaluation of the full-encirclement repairs and the patch repairs. It was unanimous that installing a patch repair on 6-inch diameter pipeline is more difficult than full-encirclement repair. Additionally, each company expressed difficulty in keeping the patch layers centered on the defect making the time

for patch installation on average 50% longer than full-encirclement repairs.

4.2 Digital Image Correlation

Digital image correlation (DIC) was performed on the external surface of the composite repair for one patch and one full-encirclement specimen from each company. DIC uses a random speckling combined with high-resolution cameras to compute strains on a component under loading.

Digital image correlation is the process by which a random speckle pattern is applied to a surface, loading applied, and the image results analyzed to determine strains developed under load. The first step in the process is to apply a coat of white paint to the surface of the component in the area of interest. In this case, white paint was applied to the exterior surface of each composite covering the defect area and extending about 3 inches in each direction. Once dry, a speckle pattern is applied to the white surface by lightly spraying black paint over the white. Care was taken to ensure the speckle image was fine enough to allow for successful image analysis, but course enough that individual speckles are visible. An example of a speckle pattern is shown in Figure 4.2.

Digital image correlation records speckle images at several pressure loads representative of a single pressure cycle. The relative position of the individual speckles is then analyzed for displacement and strains computed.

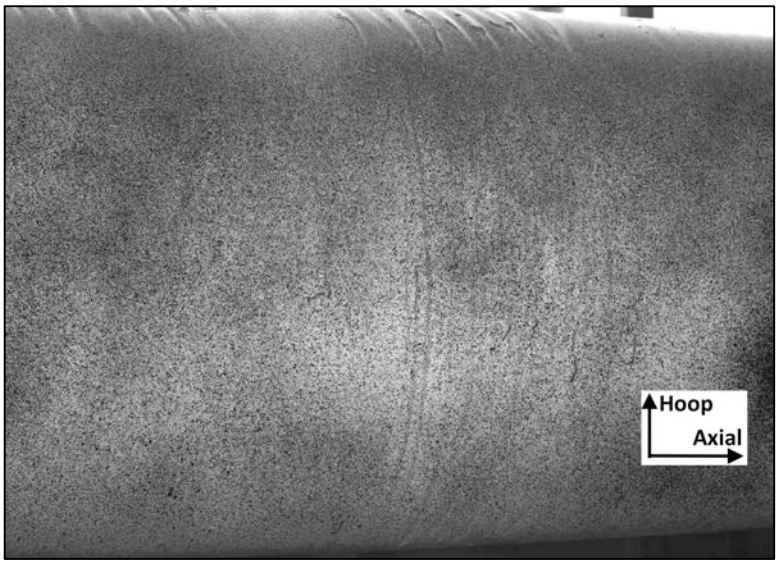

Figure 4.2: Example of a speckle pattern applied to a composite repair

To ensure speckle pattern adequacy several practice speckle patterns were sprayed onto previously failed pipe specimen. For this application, the optimal speckle spray was achieved by spraying with full power at approximately 2 feet from the component and sweeping horizontally over the entire white section.

After speckle application, each pipe was setup to receive pressure from a manually controlled pump, which allowed for better control over the applied pressure. The next step was to setup two high-resolution cameras to take images during the pressure cycle. Figure 4.3 shows a schematic of the camera setup in relation to the pipe sample.

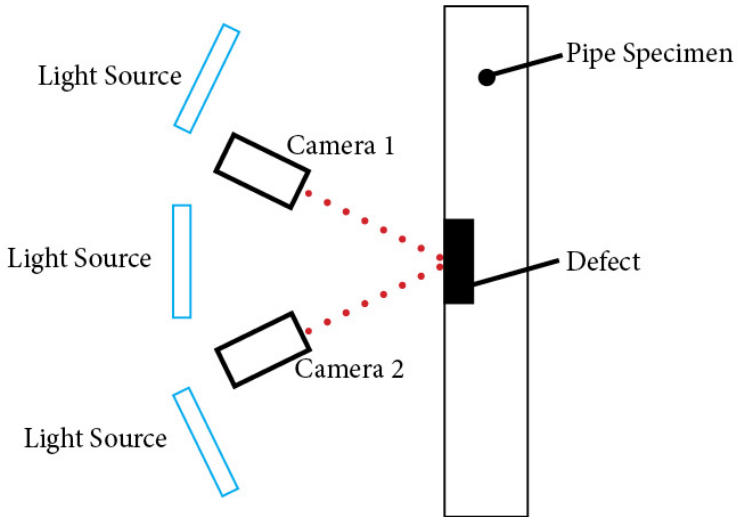

Figure 4.3: DIC setup, 2 high-resolution cameras and 3 LED light sources

Because of the nature of the test room, 3 additional light sources were necessary to achieve a useable image. Two LED lights were mounted outside and above cameras 1 and 2 while the 3rd light was mounted below and between the two cameras. This arrangement allowed for equal amounts of light on the area of interest and the best possible results from the DIC analysis.

Upon completion of the camera setup each camera was focused on the same point with a wide enough lens that they overlap the entire speckle region. This setup was critical because correlation can only be performed at the cameras overlapping views. Each camera was first rough focused at 100% zoom and then fine focused at 300% zoom. Once focused, calibration images were taken using a 9-pixel by 12-pixel grid spaced 3mm apart. Figure 4.4 shows an example of the calibration image using the calibration grid.

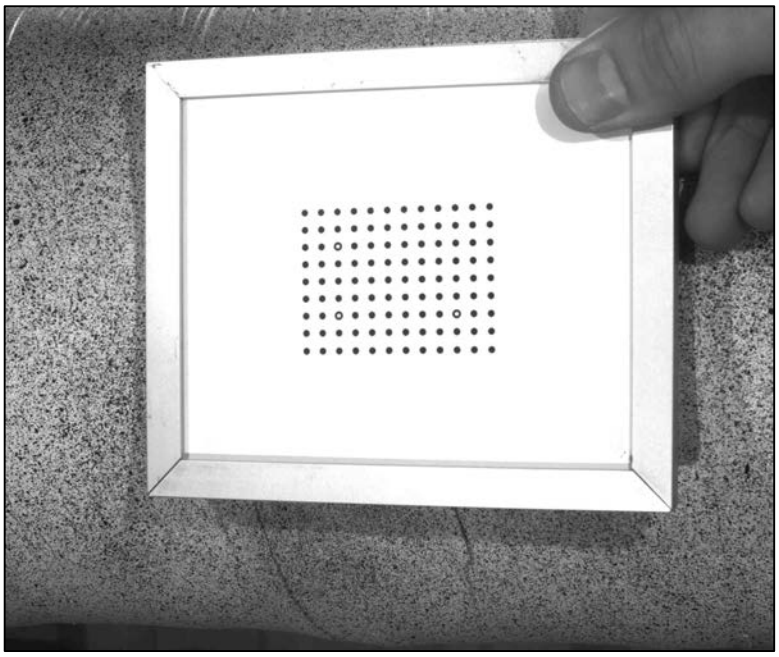

Figure 4.4: DIC calibration using a 9x12 grid

Several of these images are taken and analyzed serving as location identification between the two cameras. Once complete, the process of gathering DIC images can begin, starting with images at no pressure.

Images were taken at four intervals, 0 psi, 1000 psi, 1800 psi, and 2,130 psi, during the pressure cycles and four images were taken at each interval. Using a manually controlled pressure pump allowed for these pressures to be held constant for several seconds while recording images.

4.2.1 DIC Results

Digital image correlation outputs strain measurements in the hoop and axial directions. Figure 28 shows the DIC output for the patch repair for Company B as an example. Strains for each pipe were recorded for both the hoop and axial directions to provide comparison with the strain gauges. All DIC output for each pipe can be found in Appendix H.

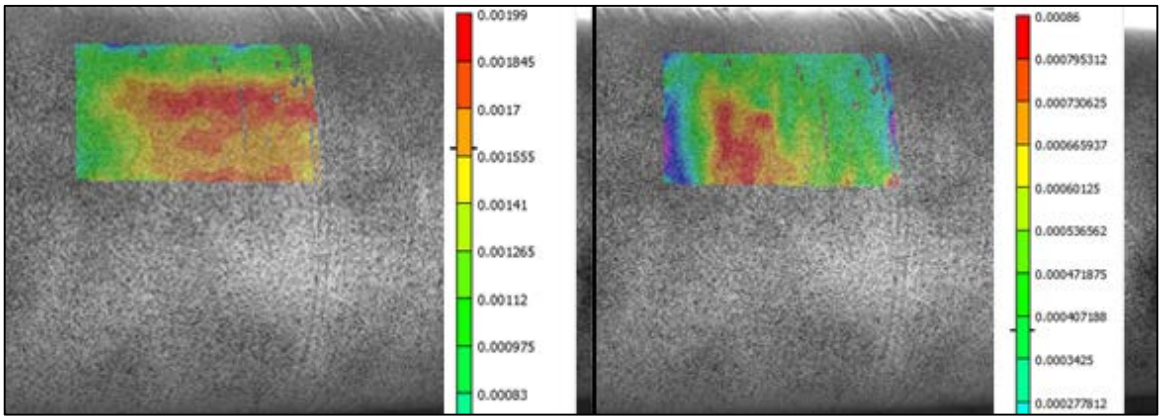

Figure 4.5: Generated DIC output for the patch repair install by Company B with hoop strains (left) and axial strains (right)

Like FEA, symmetry conditions allow for analysis to take place on ¼ of the defect area. The entire visible speckle area was first analyzed to determine which quadrant of the defect would yield the best results with minimal error. Upon identification of the section, the analysis area was refined and reanalyzed to determine strain.

The analysis was computed from the center of the defect to approximately ½-inch over the undamaged pipe section. The bottom right corner of Figure 28 is the center of the defect in both hoop and axial direction. A defect edge can be clearly seen in the hoop direction of Figure 28 with red indicating an area of high strain and the green indicating areas of lower strain. This is the transition location from the defect to the undamaged pipe section.

There are two reasons DIC was performed on these pipes. The first is to acquire a visual representation of the full-field strain developing around the defect and the second is to compare the strain values obtained from DIC with the strain values obtained from strain gauges. Figure 4.6 shows an example output from Company C's DIC analysis that was used to determine strain

values at the same locations as the strain gauges. The area shown with a black square was the location at which the strain gauges were applied and therefore strain measurements taken from DIC.

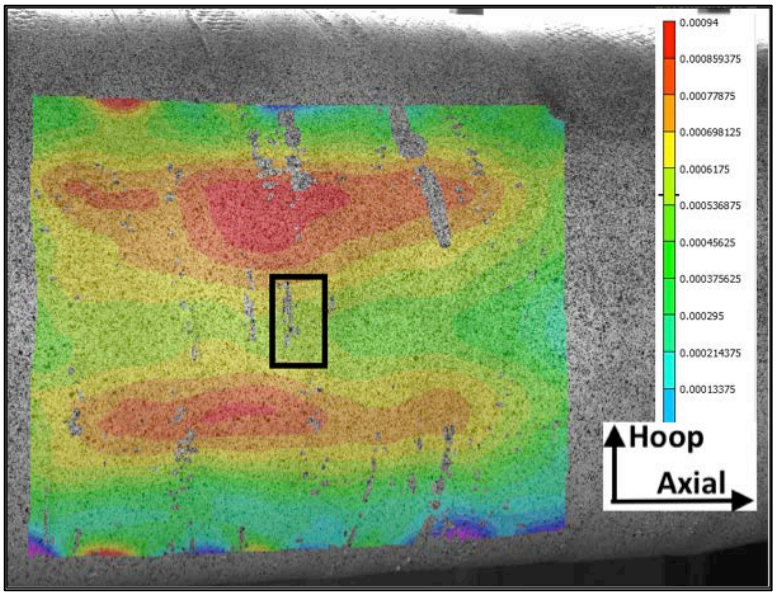

Figure 4.6: Example DIC output from Company C used to determine strains at the same locations as physical gauges. Strain measurements were taken from the black boxed region and used for comparison to strain gauges

Strain was taken from this area as an average of the overall location. Figure 4.7 shows the strain values obtained from DIC at both the location of the strain gauges as well as the maximum overall strain recorded from the DIC process.

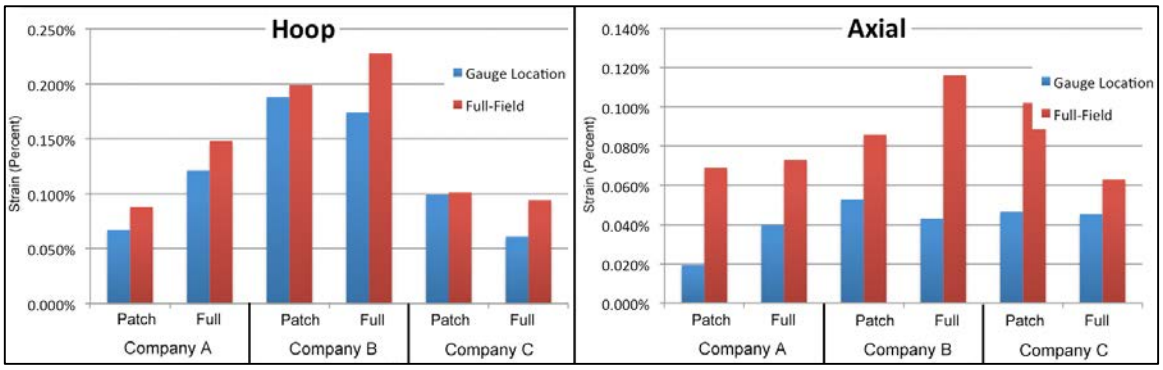

Figure 4.7: DIC strain comparison of full-field strain with strains taken at the gauge locations

The overall full-field strain was consistently greater than the strain measured at the gauge locations. This is because the full-field strain is measuring a more severe strain created by the nature of the defect. Mechanics indicates this defect could be modeled as a tensile sample. Figure 4.8 shows a simplified 2-dimensional free-body diagram of the defect in tension.

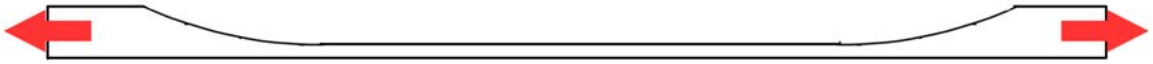

Figure 4.8: Example of the defect in tension

Modeling the defect as a flat beam under tensile load at either end is a simplified model and helps explain one of the results of DIC. Because this defect is deforming in both the axial and hoop directions, the resulting stress from this load would have stress concentrations at either edge of the defect, like the filet radii on a tensile sample.

The beam in tension analog applies well to the defect and the DIC results in Figure 4.9 help confirm this model. The high strain areas, shown in red, are the areas on either edge of the

defect where the fixed end conditions would apply. In both the hoop and the axial directions that a stress concentration exists at the edges, supporting the simple tensile beam analog.

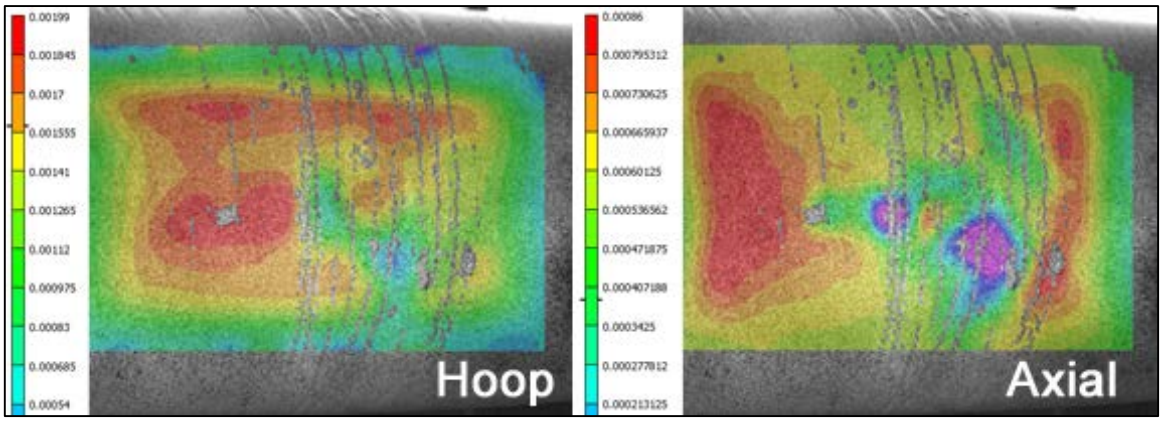

Figure 4.9: Stress concentrations on either side of the defect in both hoop (left) and axial (right) directions

4.3 Strain Gauges

4.3.1 Strain Results

Strain gauges were installed on 6 of 18 pipe samples: one full-encirclement and one patch repair from each company. The same pipes used for DIC in the above section were used for the strain gauge analysis. The gauges of interest are those installed under the repair on the surface of the defect, on the exterior surface of the repair over the defect, and on the substrate. Strain analysis consisted of looking at loop data for the beginning, middle, and end of life. This section examines the results of the strain gauges.

The average strain through the duration of life for both the patch and full-encirclement repairs for Company A are tabulated in Table 6. The maximum strain was under the repair on the surface of the defect in the hoop direction at a value of 0.2214% strain for the patch repair and 0.2690% strain for the full-encirclement repair.

Table 6: Average strain over the duration of the fatigue life for Company A

	Average Strain – Lifelong				
	Gauge 1	Gauge 2	Gauge 3	Gauge 4	Gauge 5
	Under - Hoop	Under - Axial	Outer - Hoop	Outer - Axial	Substrate
Patch	0.2214%	0.0321%	0.1349%	0.0490%	0.0726%
Full-Encirclement	0.2690%	0.0369%	0.0672%	0.0394%	0.0716%

The behavior of the strains over the lifespan of the repair was examined. A plot of beginning of life strains vs. pressure is plotted in Figure 4.10 for both patch and full-encirclement repairs. The first and the last recorded pressure cycles were analyzed for 4 pressures in each cycle.

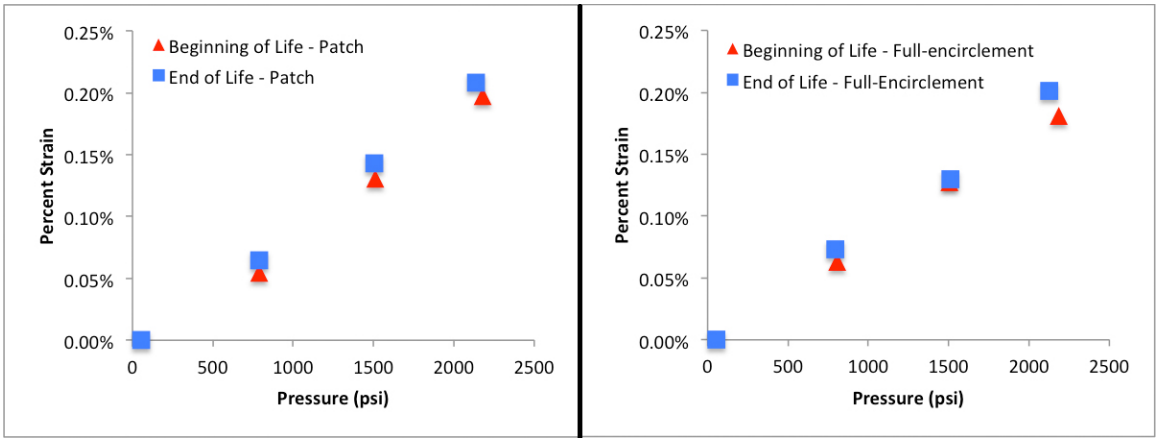

Figure 4.10: Company A - lifelong strain measurements for patch repair (left) and full-encirclement repair (right) for the hoop direction under the repair

Figure 4.10 shows that each strain increases as the fatigue cycles increase. The graphed trend is for the gauge applied on the surface of the defect, under the repair, but is consistent for all hoop strain gauges except the substrate strain, which remained nearly constant through the fatigue life. This same analysis was applied to each company and this trend remains throughout

each pipe. The greater strain at the end of fatigue life is likely due to a strain softening at the edges of the defect. This strain softening would allow for a greater displacement at the defect center, resulting in a large strain.

Table 7: Average strain over the duration of the fatigue life for Company B

	Average Strain - Lifelong				
	Gauge 1	Gauge 2	Gauge 3	Gauge 4	Gauge 5
	Under - Hoop	Under - Axial	Outer - Hoop	Outer - Axial	Substrate
Patch	0.2379%	0.0691%	0.1616%	0.0319%	0.0705%
Full-Encirclement	0.2517%	0.0429%	0.1936%	0.0590%	0.0710%

The average strain through the duration of life for both the patch and full-encirclement repairs for Company B are tabulated in Table 7. The maximum strain was under the repair on the surface of the defect in the hoop direction at a value of 0.2379% strain for the patch repair and 0.2517% strain for the full-encirclement repair.

Table 8: Average strain over the duration of the fatigue life for Company C

	Average Strain - Lifelong				
	Gauge 1	Gauge 2	Gauge 3	Gauge 4	Gauge 5
	Under - Hoop	Under - Axial	Outer - Hoop	Outer - Axial	Substrate
Patch	0.1521%	0.0507%	0.0673%	0.0468%	0.0790%
Full-Encirclement	0.1498%	0.1670%	0.1100%	0.0428%	0.0735%

The average strain through the duration of life for both the patch and full-encirclement repairs for Company C are tabulated in Table 8. The maximum strain was on the repair in the axial direction at a value of 0.1670% strain for the full-encirclement repair and under the repair

on the surface of the defect at a value of 0.1521% strain for the patch repair. Examining the hoop strains under the defect indicates that strain in the patch specimen was slightly higher than in the full-encirclement, which follows the trends indicated in FEA.

Strain values were also obtained for the substrate away from the defect, Gauge 5, and as expected strain values in the substrate remained nearly constant throughout fatigue life. The maximum difference in substrate strain was 7.3% difference for all companies.

Strains developed in the patch and full-encirclement repairs were compared to gain knowledge about repair performance. Table 9 shows strains obtained from gauges from approximately ½ the life of each pipe sample. The percent difference is given to compare each set of patch and full-encirclement repairs. All percent differences are less than 10% indicating that the strains developing in the hoop direction under the repair are similar for both repairs. A simple t-test of the patch and full-encirclement repairs results in a p-value of 0.853 meaning that from a strain analysis standpoint the repairs are statistically similar.

Table 9: Comparison of patch and full-encirclement repairs

Percent Difference Patch and Full-Encirclement Repairs			
Company	Repair Type	Under - Hoop	Percent Difference
A	Patch	0.2323%	+8.061%
A	Full-Encirclement	0.2143%	
B	Patch	0.2331%	-3.250%
B	Full-Encirclement	0.2408%	
C	Patch	0.1601%	+7.316%
C	Full-Encirclement	0.1488%	

4.3.2 Strain and DIC Comparison

Strain measurements at MAOP from the first pressure cycle were compared with DIC measurements at MAOP. Figure 4.11 shows the resulting strain values for each company and each repair.

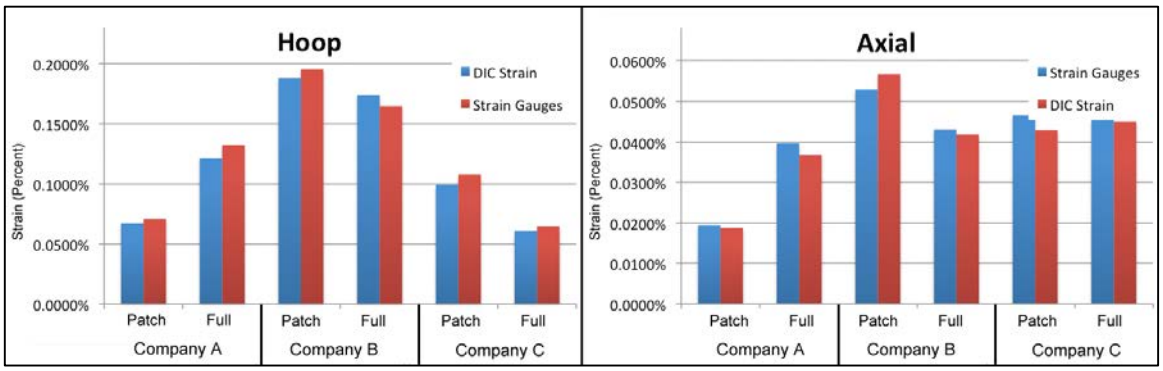

Figure 4.11: Comparison of DIC strain and strain from gauges

DIC and strain gauges were similar, but DIC measured consistently larger strain than strain gauges. This difference in strain is likely a result of edge effects in the DIC analysis.

4.4 Large-Scale Fatigue Results

As expected, the fatigue cycle rates for the large specimens were significantly slower than for the small-scale specimens. This necessitated attempting to run the system 24 hours to reduce the overall time required for the test. While this approach was making progress, at around 20,000 cycles the head on the valve side of the pressure vessel developed a crack. This crack was in the "knuckle" region of the vessel, where the stresses are the highest and weld-repairs are typically ineffective. While the stress analysis indicates that the vessel was safe for the applied internal pressure, the additional hammering caused by the depressurization when the solenoid valves opened likely caused the failure. This assumption was reinforced when a related test system using a nearly identical vessel and fatigue setup developed a crack in the same region. The

vessel was drained and then weld repaired and then testing was resumed. The crack propagated again after approximately 4000 cycles. The vessel has been repaired again and testing is ongoing. The current cycles on the test vessel is 26,268 cycles.

While the test has not yet reached runout, we can make one critical observation. Company A applied the same type of repair on the large-scale specimen as they did on the small-scale specimen, with respect to repair thickness and overlap. At this point, we have exceeded their small-scale performance by a factor of almost four. Performance improvement of this magnitude is unlikely the result simple scatter and is likely due to the underlying mechanics of the system. The internal pressure for achieving 72% SYMS in a 42-inch vessel was only 500 psi. The failures in the small-scale specimens occurred in the transition region between the undamaged section and the thinned section. Based on the stress analysis of the damaged region, the interior edge of this transition region is the region of highest tensile stress and strain, which is reinforced by the DIC results. This region is loaded in two ways. The first loading is the simple hoop and axial stresses due to the internal pressure in the vessel. The second loading is due to the out-of-plane deflection of the thinned region. In the large-scale specimen, this out-of-plane deflection is significantly less since the internal pressures are less than 25% of the small-scale specimens. This reduction in deflection will reduce the stresses in the transition region and should lead to increased fatigue life. This is a critical observation since this implies that testing, at least for machined simulated corrosion defects, on small scale specimens is likely more stringent than large scale specimens at similar hoop and axial stress levels.

5 CONCLUSIONS AND RECOMMENDATIONS

A combination of computational and experimental study was performed to investigate the behavior of patch and full-encirclement repairs. Results from the FEA simulations indicated that the underlying substrate strains in both patch and full-encirclement repairs were similar. However, this did not hold for the strain within the composite material. Strains in patch repairs were found to be greater than the full-encirclement repairs for defects with less than 55% wall loss and less for defects greater than 55% wall loss. Strain levels in the composite repair were found to be insensitive to the extent of the repair past the minimum required by PCC – 2. This was true for both the full encirclement and patch repairs.

Fatigue cycle testing was then performed to compare the performance of patch and full-encirclement bonded composite repairs. A total of 18 pipes, each with a 75% machined wall loss defect, were repaired, 9 with patch repairs and 9 with full-encirclement repairs. This performance testing indicated that patch repairs lasted, on average, 3.9 times longer than full-encirclement repairs. Based on this experimental data, it can be concluded that patch repairs are a viable option for 6-inch steel pipeline with wall loss defects. The large-scale test is still ongoing, but based on the current results, it appears that the performance of a composite repair on a small-scale test vessel will accurately predict the performance of the repair on a large-scale vessel as well.

The performance difference between full-encirclement and patch repairs was unexpected, but may be the result of the additional substrate deformation that is allowed in patch repairs. FEA indicated that the substrate bulges some in the gap between repair edges, which could allow for a reduction in strain at the top of the repair. Further study is required to fully understand the role of non-symmetric deformation effects on repair life.

Based on this research, patch type repairs are a viable option for the rehabilitation of damaged pressure equipment and pipelines. These repair types have, at least, similar performance to full encirclement repairs and appear to have excellent fatigue performance. If the repair thicknesses are chosen appropriately, these repairs can withstand 100,000 pressure cycles without failure. The current guidance for the size of the lateral extent of the repair, L_{over}, in ASME PCC-2 appears to be sufficient to provide reliable patch repairs for external corrosion.

6 BIBLIOGRAPHY

[1] A. Mohitpour, Mo Golshan, H Murray, *Pipeline Design & Construction: A Practical Approach*, 2nd ed. American Society of Mechanical Engineers, 2003.

[2] M. D. Chapetti, J. L. Otegui, C. Manfredi, and C. F. Martins, "Full Scale Experimental Analysis of Stress States in Sleeve Repairs of Gas Pipelines," *Int. J. Press. Vessel. Pipeing*, vol. 78, pp. 379–387, 2001.

[3] G. Jacobson, "Corrosion - A Natural but Controllable Process," *National Association of Corrosion Engineers*, 2015. .

[4] C. I. Ossai, B. Boswell, and I. J. Davies, "Pipeline failures in corrosive environments - A conceptual analysis of trends and effects," *Eng. Fail. Anal.*, vol. 53, pp. 36–58, 2015.

[5] G. Kock, M. Brongers, N. Thompson, Y. Virmani, and J. Payer, "Corrosion costs and preventive strategies in the United States."

[6] C. W. Burnworth and M. W. Keller, "Performance of Patch and Full-Encirclement Bonded Composite Repairs," *Mech. Compos. Multi-functional Mater.*, vol. 7, pp. 337–343, 2015.

[7] A. R. Mableson, K. R. Dunn, N. Dodds, and A. G. Gibson, "Refurbishment of Steel Tubulars using Composite Materials," *Plast. Rubber Compos.*, vol. 29, no. 10, pp. 558–565, 2000.

[8] C. Greenwood, "Composite Pipe Repair Method Shows Versatility, Long-Lasting," *Pipeline Gas J.*, vol. 228, no. 2, p. 58, 2001.

[9] C. R. Alexander and F. D. Wilson, "Development and testing of the armor plate pipeline repair system," 1997.

[10] W. R. True, "Composite wrap approved for U.S. gas-pipeline repairs," *Oil&Gas J.*, vol.

93, no. 41, 1995.

[11] P. Smith and J. Cuthill, “Patching up pipework with carbon-fiber composites,” *Mater World*, vol. 10, no. 5, p. 28, 2002.

[12] N. A. of C. Engineers, “Joint Surface Preparation Standard,” 2000.

[13] J. M. Wilson, “Characterization of a Carbon Fiber Reinforced Polymer Repair System for Structurally Deficient Steel Pipeing," 2006.

[14] J. M. Duell, “Characterization and FEA of a Carbon Composite Overwrap Repair System," University of Tulsa, 2004.

[15] ASTM, “PCC-2,” pp. 139–184, 2011.

APPENDIX A FEA MATERIAL MODELS

The following material models were used in the FEA simulations. These values correspond to the material models used for FEA in chapter 2.

Table 10: FEA material properties - steel substrate

Steel Substrate Material Properties		
Elastic Properties	Modulus of Elasticity (psi)	Poisson's Ratio
	30,000,000	0.30
Plastic Properties	Yield Stress (psi)	Plastic Strain (in/in)
	41000	0
	41300	0.003395
	44400	0.007734
	47600	0.012213
	50800	0.016268
	54200	0.019878
	57500	0.024347
	61000	0.031909
	64800	0.043747
	69100	0.061653
	73600	0.081793
	82200	0.1695

Table 11: FEA material properties - composite

Composite Repair - Carbon Fiber Composite		
E1	7,130,000	psi
E2	3,460,000	
E3	3,460,000	
Nu12	0.196	
Nu13	0.196	
Nu23	0.196	
G12	88,780	psi
G13	88,780	
G23	88,780	

Table 12: FEA material properties - putty

Restoration Putty	
Modulus of Elasticity	252,000
Poisson's Ratio	0.28

APPENDIX B DETAILED MESH IMAGES

The following images are detailed images of the mesh used in FEA simulations.

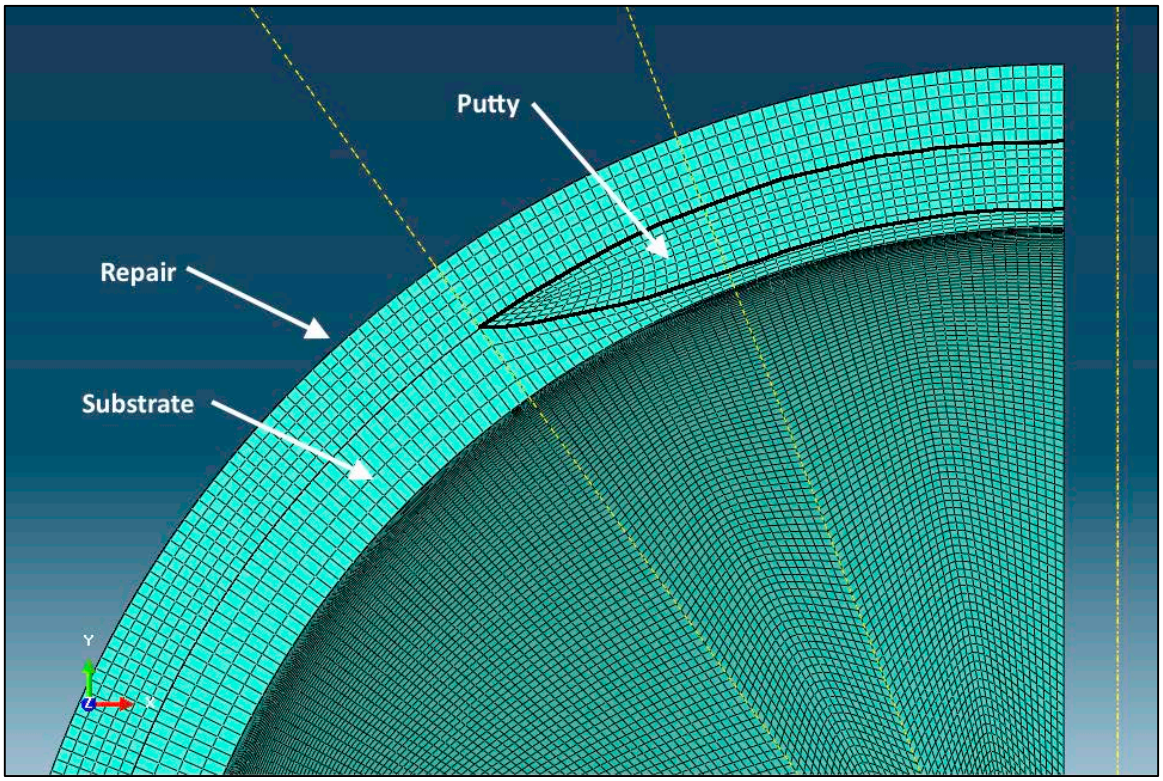

Figure 6.1: Front View – Putty material outlined in black

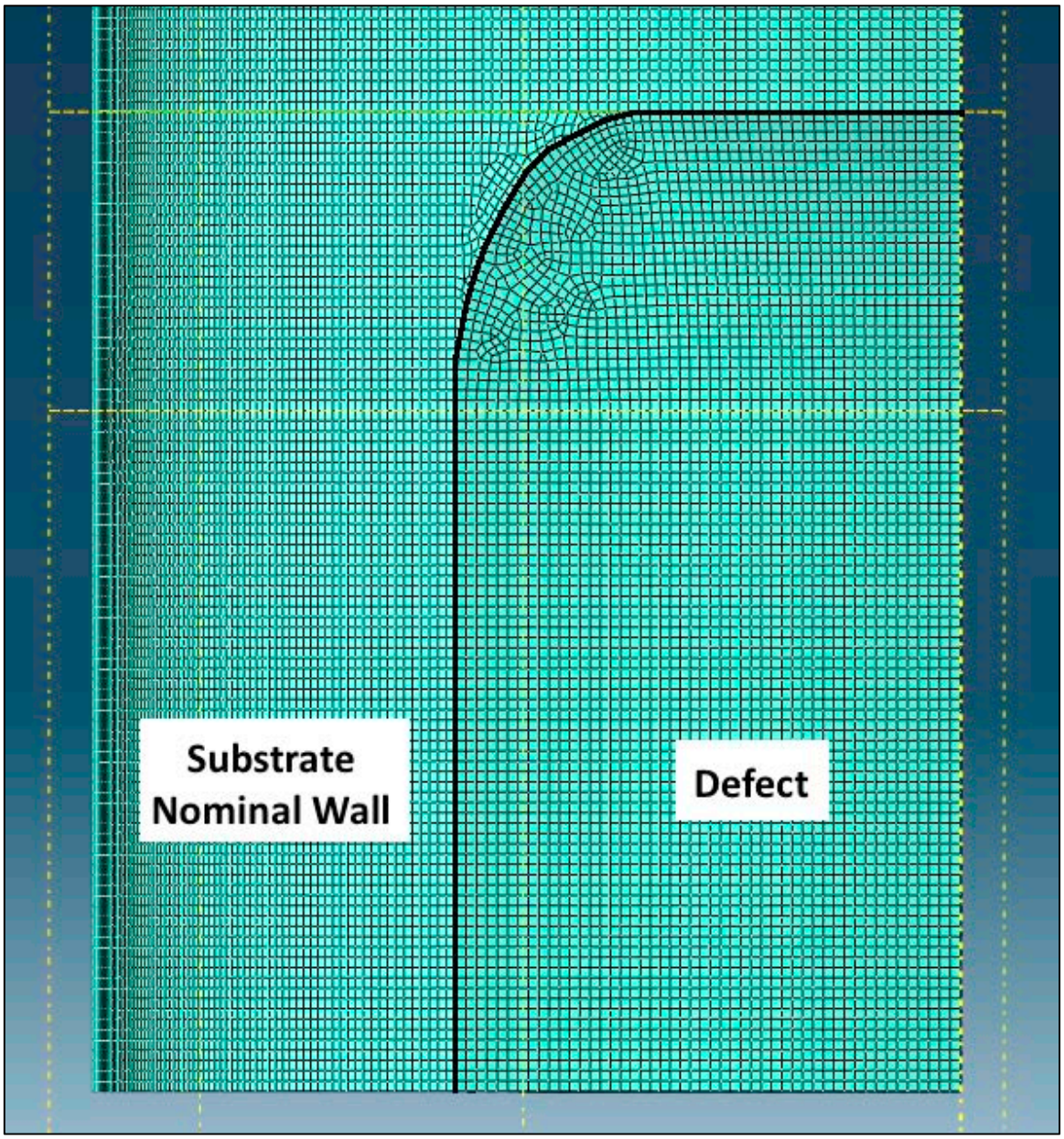

Figure 6.2: Top View – Substrate only, defect location outlined in black.

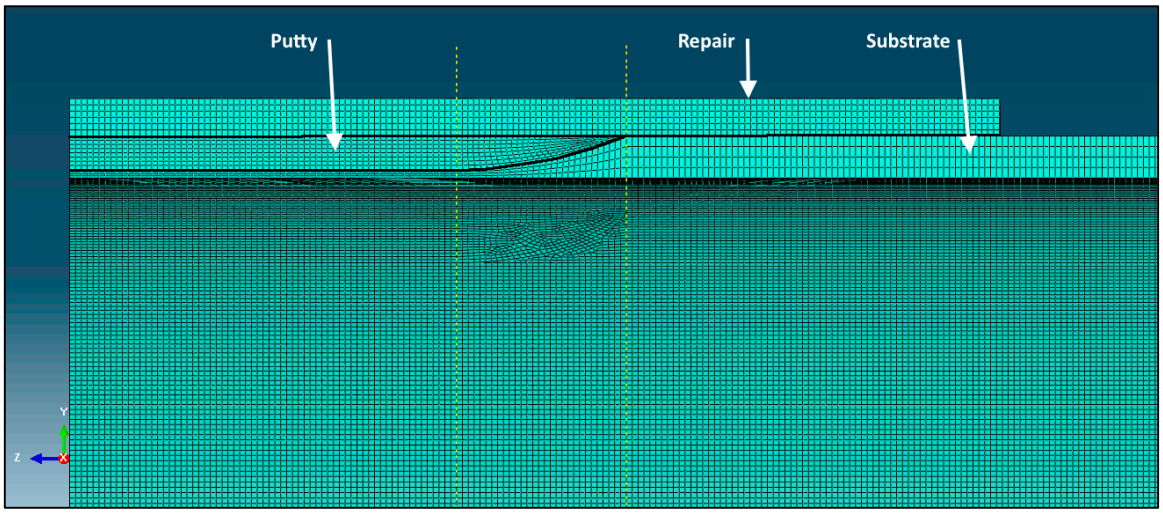

Figure 6.3: Side View – Putty material outlined in black.

APPENDIX C TABULATED MESH CONVERGENCE VALUES

The following values are the tabulated results from FEA. They correspond to the mesh convergence study performed in Chapter 2.

Table 13: Mesh convergence values

Global Seed Size	Pressure (psi)	Mises Max Stress (psi)	Max Principal Stress (psi)
5	100	3138	3538
4	100	3150	3552
3	100	3199	3607
2	100	3401	3844
1	100	3531	3992
0.85	100	3593	4063
0.75	100	3680	4160
0.65	100	3680	4160
0.55	100	3680	4160

Global Seed Size	Local Seed Size*	Pressure (psi)	Mises Max Stress (psi)	Max Principal Stress (psi)
2.5	0.75	100	3680	4160

*Local seeds were taken to be at all edges of the defect area.

APPENDIX D TABULATED DATA FOR WALL LOSS

The following data corresponds to the wall loss study performed in chapter 2. Values highlighted in red indicate substrate undergoing plastic deformation.

Table 14: Tabulated FEA values for percent wall loss

	Wall Loss	Substrate		Repair	
		Max Strain (in/in)	Max Stress (psi)	Max Strain (in/in)	Max Stress (psi)
Full- Encirclement	50%	1.362E-03	41000	6.040E-03	8247
	55%	1.633E-03	41030	6.832E-03	10150
	60%	2.235E-03	41090	7.772E-03	11340
	65%	3.593E-03	41230	8.910E-03	13480
	70%	5.342E-03	42140	1.100E-02	16500
	75%	5.947E-03	42620	1.315E-02	20210
Patch	50%	1.344E-03	40700	6.179E-03	14230
	55%	1.599E-03	41020	6.903E-03	15870
	60%	2.168E-03	41080	7.753E-03	17880
	65%	3.490E-03	41220	8.796E-03	20360
	70%	5.382E-03	42170	1.063E-02	25080
	75%	5.978E-03	42640	1.257E-02	30260

APPENDIX E THICKNESS MEASUREMENTS POST-MACHINING

An ultrasonic tester was used to determine thickness of the defect after the machining process. A series of measurements were taken: 9 measurements on the defect, 3 on the substrate. These measuring locations are outlined below and the resulting values are tabulated. Target thickness was 0.07 inches, which corresponds to a 75% wall loss.

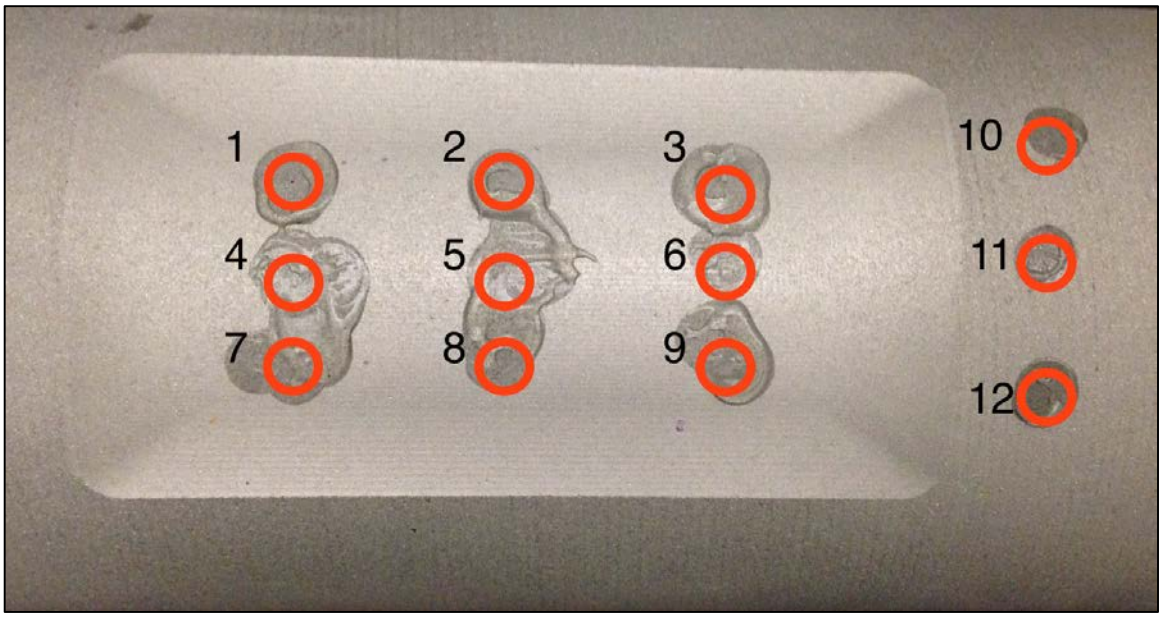

Figure 6.4: Thickness measurement locations

Table 15: Measured thicknesses for each pipe sample

Defect Thickness Measurements									Substrate Thickness		
1	**2**	**3**	**4**	**5**	**6**	**7**	**8**	**9**	**10**	**11**	**12**
0.069	0.075	0.090	0.071	0.070	0.077	0.070	0.066	0.092	0.302	0.270	0.292
0.080	0.084	0.071	0.094	0.086	0.093	0.076	0.066	0.066	0.313	0.280	0.275
0.093	0.094	0.076	0.077	0.068	0.076	0.085	0.092	0.094	0.275	0.300	0.311
0.081	0.075	0.071	0.092	0.068	0.092	0.080	0.082	0.089	0.315	0.282	0.309
0.081	0.095	0.068	0.095	0.093	0.081	0.068	0.076	0.072	0.285	0.270	0.288
0.086	0.088	0.086	0.073	0.082	0.091	0.075	0.091	0.084	0.316	0.298	0.278
0.088	0.074	0.089	0.070	0.070	0.094	0.076	0.074	0.091	0.293	0.266	0.291
0.086	0.088	0.070	0.069	0.082	0.095	0.075	0.095	0.080	0.289	0.272	0.305
0.085	0.085	0.071	0.085	0.094	0.067	0.071	0.079	0.066	0.275	0.278	0.291
0.079	0.088	0.076	0.082	0.080	0.077	0.089	0.089	0.092	0.315	0.274	0.303
0.083	0.067	0.079	0.081	0.065	0.074	0.085	0.092	0.079	0.307	0.275	0.296
0.085	0.068	0.084	0.095	0.082	0.071	0.074	0.095	0.091	0.297	0.277	0.299
0.089	0.073	0.093	0.078	0.070	0.068	0.069	0.078	0.091	0.286	0.307	0.298
0.083	0.091	0.083	0.089	0.069	0.081	0.093	0.069	0.085	0.287	0.271	0.309
0.084	0.091	0.084	0.085	0.067	0.069	0.090	0.088	0.069	0.297	0.274	0.298
0.082	0.089	0.083	0.073	0.070	0.079	0.084	0.091	0.077	0.290	0.275	0.284
0.093	0.084	0.086	0.072	0.093	0.069	0.088	0.072	0.084	0.288	0.272	0.311
0.076	0.088	0.090	0.092	0.095	0.065	0.073	0.086	0.089	0.298	0.282	0.296

APPENDIX F FATIGUE DATA AND COMPUTED P-VALUES

Cycles to failure and computed t-test statistics are tabulated. T-test statistics are based on a 2-tailed test with a confidence of $\alpha = 0.05$.

Table 16: Cycles to failure

	Type of Repair	Cycles to Failure	Strain Gauge?
Company A	Patch	2,560	Yes
		748	No
		5,631	No
	Full-encirclement	5,798	Yes
		2,253	No
		946	No
	Average Cycles	2,989	Cycles
	Standard Deviation	2033	Cycles
	T-Test (p-value)	0.993	Statistically Similar
Company B	Patch	34,286	Yes
		100,000 r	No
		100,000 r	No
	Full-encirclement	1,605	Yes
		17,377	No
		21,147	No
	Average Cycles	45,736	Cycles
	Standard Deviation	39532	Cycles
	T-Test (p-value)	0.089	Statistically Similar
Company C	Patch	23,371	Yes

		100,000 r	No
		100,000 r	No
	Full-encirclement	26,750	Yes
		20,536	No
		22,940	No
	Average Cycles	48,933	Cycles
	Standard Deviation	36155	Cycles
	T-Test (p-value)	0.183	Statistically Similar

* Cycles reaching runout are designated: “100,000 r”

APPENDIX G DIGITAL IMAGE CORRELATION

The following images supplement the DIC images in Chapter 4. They are broken down by company with one hoop and one axial image for the patch repair and full-encirclement repair.

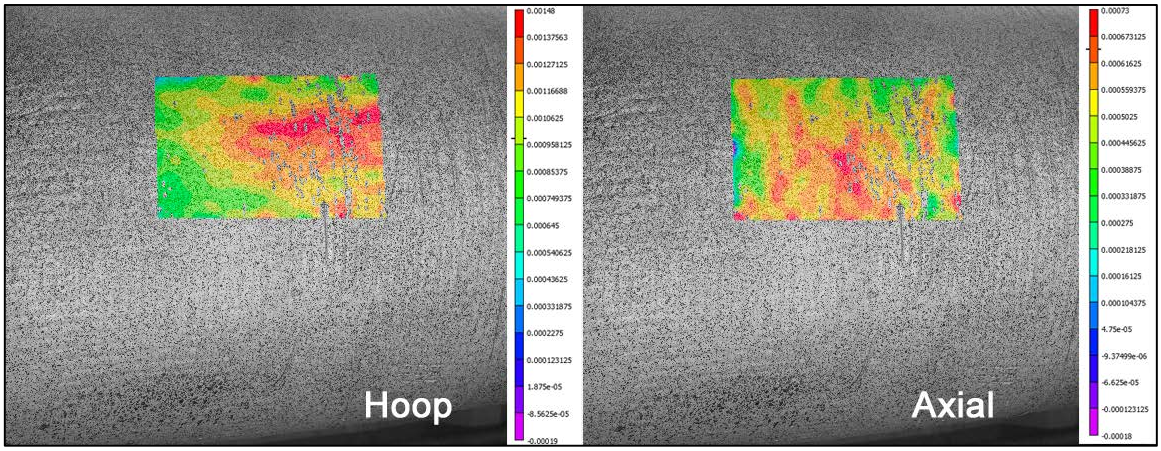

Figure 6.5: Company A – Full-encirclement Repair:

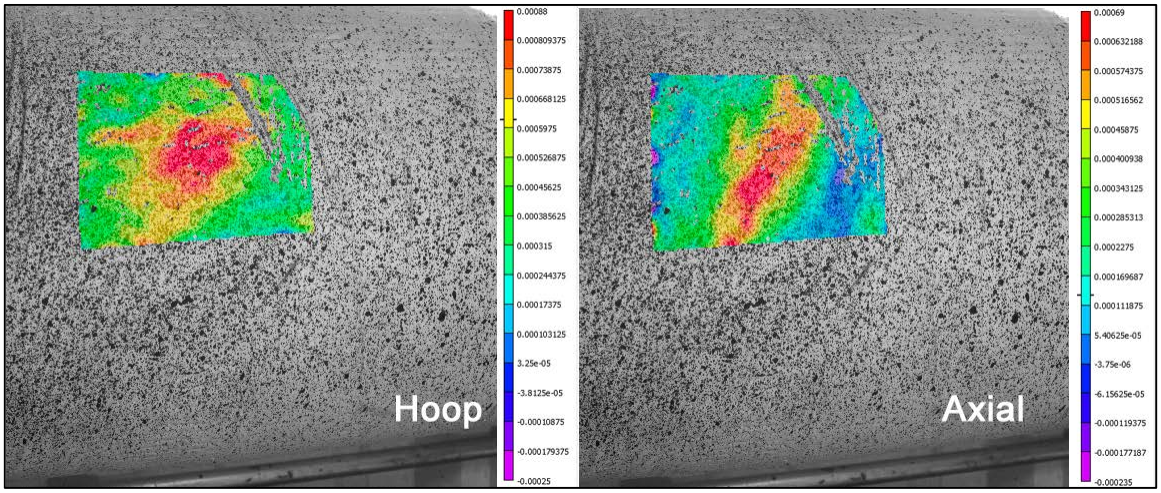

Figure 6.6: Company A – Patch Repair:

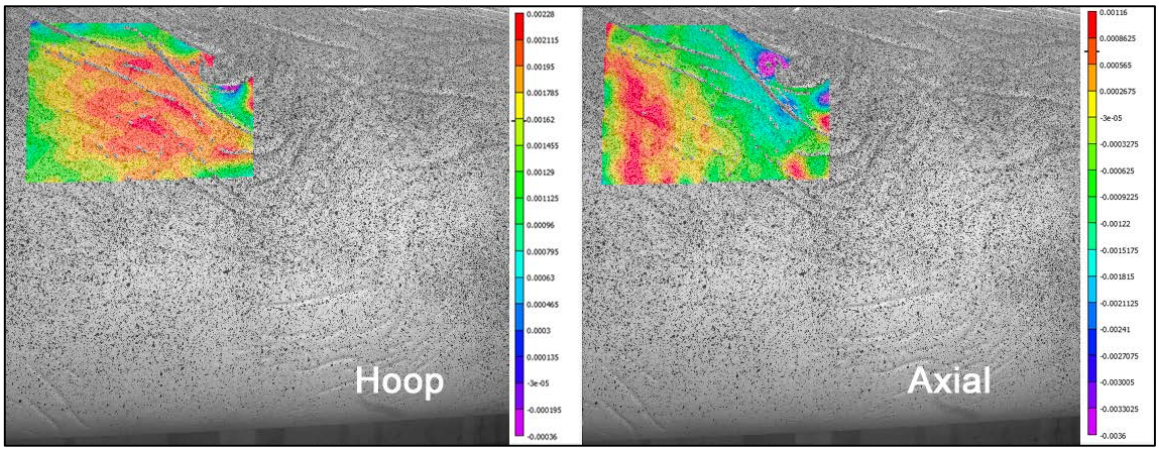

Figure 6.7: Company B – Full-encirclement Repair:

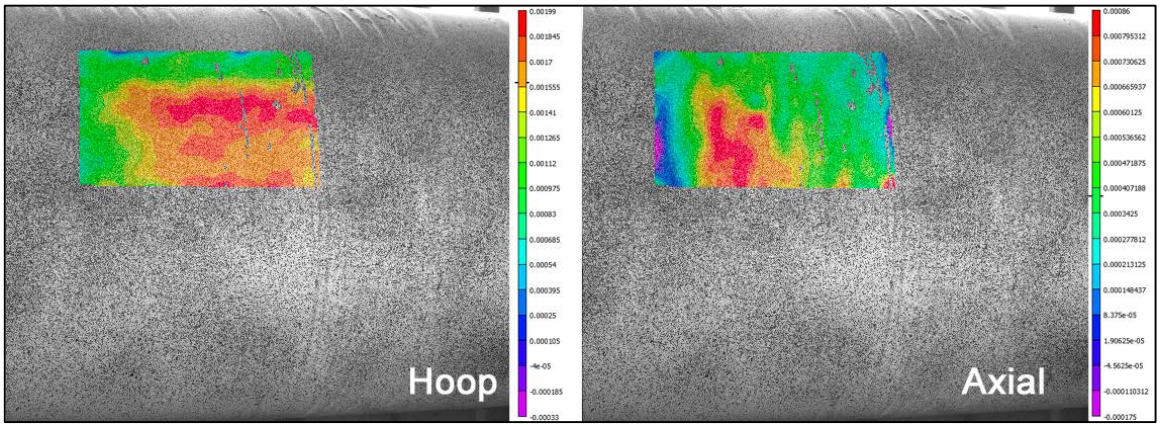

Figure 6.8: Company B – Patch Repair:

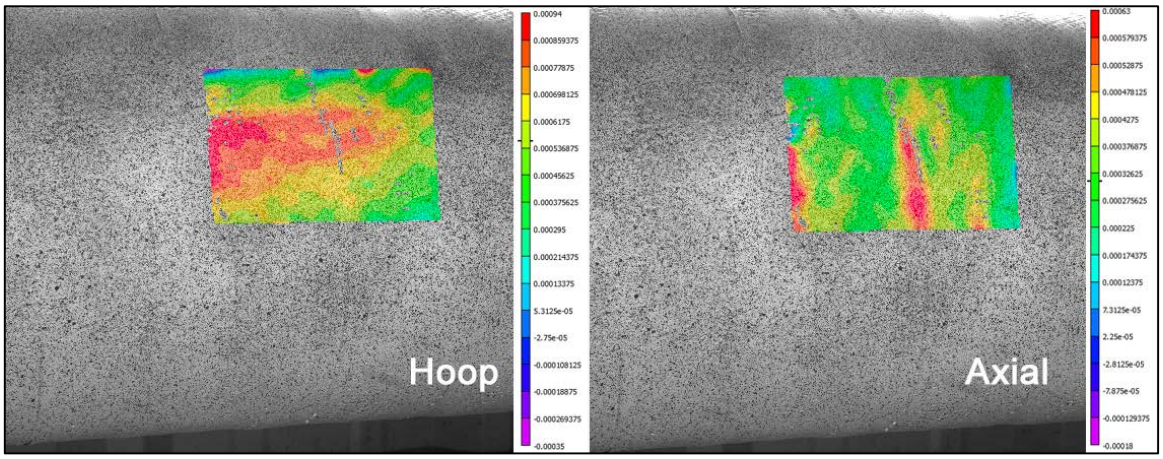

Figure 6.9: Company C – Full-encirclement Repair:

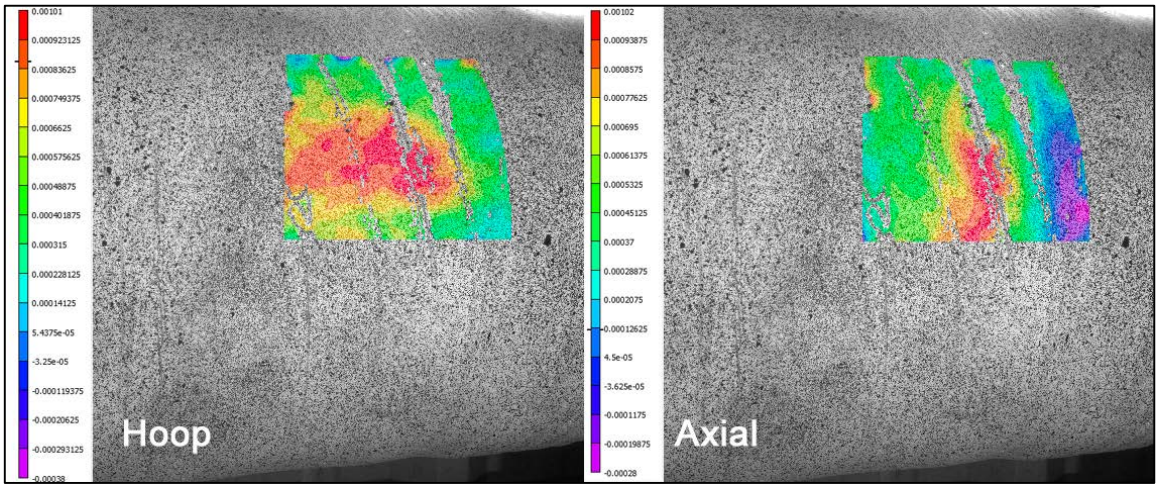

Figure 6.10: Company C – Patch Repair: